1 **Mitotic chromosomes scale to nucleo-cytoplasmic ratio and cell size in *Xenopus***

2

3 Coral Y. Zhou[1], Bastiaan Dekker[2], Ziyuan Liu[1], Hilda Cabrera[1], Joel Ryan[3], Job Dekker[2,4],

4 Rebecca Heald[1]

5

6 [1]Department of Molecular and Cell Biology, University of California, Berkeley, Berkeley, CA,

7 USA; [2]Department of Systems Biology, University of Massachusetts Chan Medical School,

8 Worchester, MA, USA; [3]Advanced BioImaging Facility, McGill University, Montreal, Quebec, CA

9 [4]Howard Hughes Medical Institute, Chevy Chase, MD, USA.

10

11 Correspondence:

12 Coral Zhou: coral.zhou@berkeley.edu

13 Rebecca Heald: bheald@berkeley.edu

14

15

16 **Abstract**

17 During the rapid and reductive cleavage divisions of early embryogenesis, subcellular structures

18 such as the nucleus and mitotic spindle scale to decreasing cell size. Mitotic chromosomes also

19 decrease in size during development, presumably to coordinately scale with mitotic spindles, but

20 underlying mechanisms are unclear. Here we combine *in vivo* and *in vitro* approaches using eggs

21 and embryos from the frog *Xenopus laevis* to show that mitotic chromosome scaling is

22 mechanistically distinct from other forms of subcellular scaling. We found that mitotic

23 chromosomes scale continuously with cell, spindle and nuclear size *in vivo*. However, unlike for

24 spindles and nuclei, mitotic chromosome size cannot be re-set by cytoplasmic factors from earlier

25 developmental stages. *In vitro*, increasing nucleo-cytoplasmic (N/C) ratio is sufficient to

26 recapitulate mitotic chromosome scaling, but not nuclear or spindle scaling, through differential

27 loading of maternal factors during interphase. An additional pathway involving importin α scales

28 mitotic chromosomes to cell surface area/volume (SA/V) during metaphase. Finally, single-

29 chromosome immunofluorescence and analysis of Hi-C data suggest that mitotic chromosomes

30 scale through decreased recruitment of condensin I, resulting in major rearrangements of DNA

31 loop architecture to accommodate the same amount of DNA on a shorter axis. Together, our

32 findings demonstrate how mitotic chromosome size is set by spatially and temporally distinct

33 developmental cues in the early embryo.

34

35

36

37

38

39

40

Introduction

Upon fertilization, embryos undergo a series of rapid cell division events in the absence of cell growth, thereby decreasing cell size. Subcellular structures including the nucleus and mitotic spindle scale to cell size through a set of defined mechanisms (Heald and Gibeaux, 2018; Levy and Heald, 2015). Mitotic chromosomes also shrink in size during development and scale with cell size across metazoans (Kramer et al., 2021; Micheli et al., 1993), but underlying mechanisms are poorly understood. In plants and in fly embryos, artificially lengthening chromosomes resulted in increased chromosome mis-segregation during mitosis (Schubert and Oud, 1997; Sullivan et al., 1993). Similar experiments in budding yeast showed that the artificially longer chromosome was hyper-compacted during anaphase due to Aurora B kinase phosphorylation of substrates including condensin, a key regulator of mitotic chromosome condensation and resolution (Neurohr et al., 2011). In *C. elegans*, a genetic screen for genes required for segregation of an extra-long chromosome identified the centromeric histone CENP-A and topoisomerase II (topo II) as regulators of holocentric chromosome size (Ladouceur et al., 2017). However, it is unclear whether pathways that tune the length of an artificially long chromosome also operate during the physiological process of mitotic chromosome scaling during embryogenesis.

Mechanisms that scale the spindle and nucleus during development have been well-characterized. As cell volume decreases, structural components become limiting (Good et al., 2013; Hazel et al., 2013). In addition, some scaling factors are regulated by the nuclear transport factor importin α, which partitions between the cytoplasm and the cell membrane and serves as a sensor for the cell surface area to volume ratio (Brownlee and Heald, 2019). Previous studies of mitotic chromosome scaling, performed mainly in *C. elegans,* revealed that mitotic chromosome size correlates positively with cell size and nuclear size and negatively with intranuclear DNA density (Hara et al., 2013; Ladouceur et al., 2015). Knockdown of importin α or

3

66   the chromatin-bound Ran guanine exchange factor RCC1 decreased both nuclear and mitotic

67   chromosome size (Hara et al., 2013; Ladouceur et al., 2015). Haploid embryos generated by

68   katanin knockdown contained longer mitotic chromosomes compared to diploids (Hara et al.,

69   2013). However, conserved relationships among genome size, nuclear size, and cell size

70   complicate efforts to distinguish correlation from causation of mitotic chromosome scaling.

71   Furthermore, it is unclear whether similar underlying mechanisms operate during embryogenesis

72   of vertebrates that possess larger chromosomes and more complex karyotypes.

73

74   The African clawed frog *Xenopus laevis* provides a powerful system for studying mechanisms of

75   mitotic chromosome scaling. Female frogs produce thousands of eggs that enable isolation of

76   undiluted and cell cycle-synchronized cytoplasm in the form of egg extracts that reproduce many

77   cellular processes *in vitro* including mitotic chromosome condensation (Maresca and Heald,

78   2006). In addition, fertilized eggs divide synchronously allowing extracts to be prepared from

79   embryos at different stages of development. Our previous work demonstrated that egg extracts

80   can recapitulate a decrease in chromosome size between early and late blastula stages of

81   development *in vitro* (Kieserman and Heald, 2014)*,* but did not uncover underlying scaling

82   mechanisms. Here, we fully leverage the *Xenopus* system by systematically comparing changes

83   in mitotic chromosome size observed *in vivo* with perturbations *in vitro* to distinguish factors that

84   regulate mitotic chromosome scaling including nuclear size, spindle size, cell size, cell-cycle stage

85   and nucleo-cytoplasmic (N/C) ratio. We find that mitotic chromosomes scale continuously with

86   spindle size, even in large cells of the early embryo. We show that scaling occurs primarily through

87   differential recruitment of the DNA loop extruding motor condensin I, which alters DNA loop size

88   and thus length-wise compaction of chromosomes. Finally, we describe how two distinct

89   developmental cues, cell size and nucleocytoplasmic ratio, combine to reduce chromosome

90   length over the course of development. Together, these results create a multi-scale model for

91   how mitotic chromosome size is set in the embryo and open up new avenues for deeper

92   exploration of how changes in chromosome size and architecture contribute to early vertebrate

93   embryogenesis.

94

95   **Results**

96   **Mitotic chromosomes scale continuously with cell, nuclear, and spindle size.**

97   We reasoned that mitotic chromosome size may relate to nuclear size and content due to factors

98   associated with the DNA prior to entry into mitosis, such as histones. Alternatively, mitotic

99   chromosomes could scale with spindle size through mechanisms operating in mitosis. To

100   distinguish between these possibilities, we performed a time course of whole embryo

101   immunofluorescence through the late blastula stages of *X. laevis* development and measured the

102   dimensions of cells, spindles, and metaphase plates (Figure 1A-B). Although previous work

103   showed that spindle lengths reach a plateau in cells larger than ~200 microns in diameter (Figure

104   1-S1A, (Wühr et al., 2008)), measurement of spindle volumes by confocal microscopy revealed

105   size scaling in cells as large as 600 microns in diameter (Figure 1C), consistent with observations

106   that spindle width correlates more robustly with cell volume than spindle length in cultured cells

107   (Figure 1-S1B, (Kletter et al., 2021). Mitotic chromosome volumes also scaled continuously with

108   cell size, similar to published work describing nuclear scaling (Figure 1D, Figure 1-S2, (Jevtić and

109   Levy, 2015)). To assess whether mitotic chromosomes scale more with nuclear size or with mitotic

110   spindle size, we binned the data by cell size and plotted average volumes of the different

111   subcellular structures. We found that mitotic chromosomes scaled remarkably well with both

112   spindles and nuclei (Figure 1-S3). However, the magnitude change in nuclear volume was far

113   greater than for mitotic structures: nuclei scaled by ~10-fold over early cleavage divisions, while

114   mitotic chromosomes and spindles scaled by 3-fold and 2-fold, respectively (Figure 1E-F). Thus,

115   the change in chromosome compaction as cells enter mitosis diminishes from 8-fold in early

116   blastula embryos to 1.5-fold in late blastula stages (Figure 1-S4). Overall, these results

117   demonstrate that mitotic chromosomes scale continuously with cell size in the early embryo and

118   suggest that mitotic chromosomes may share scaling features with both nuclei and mitotic

119   spindles.
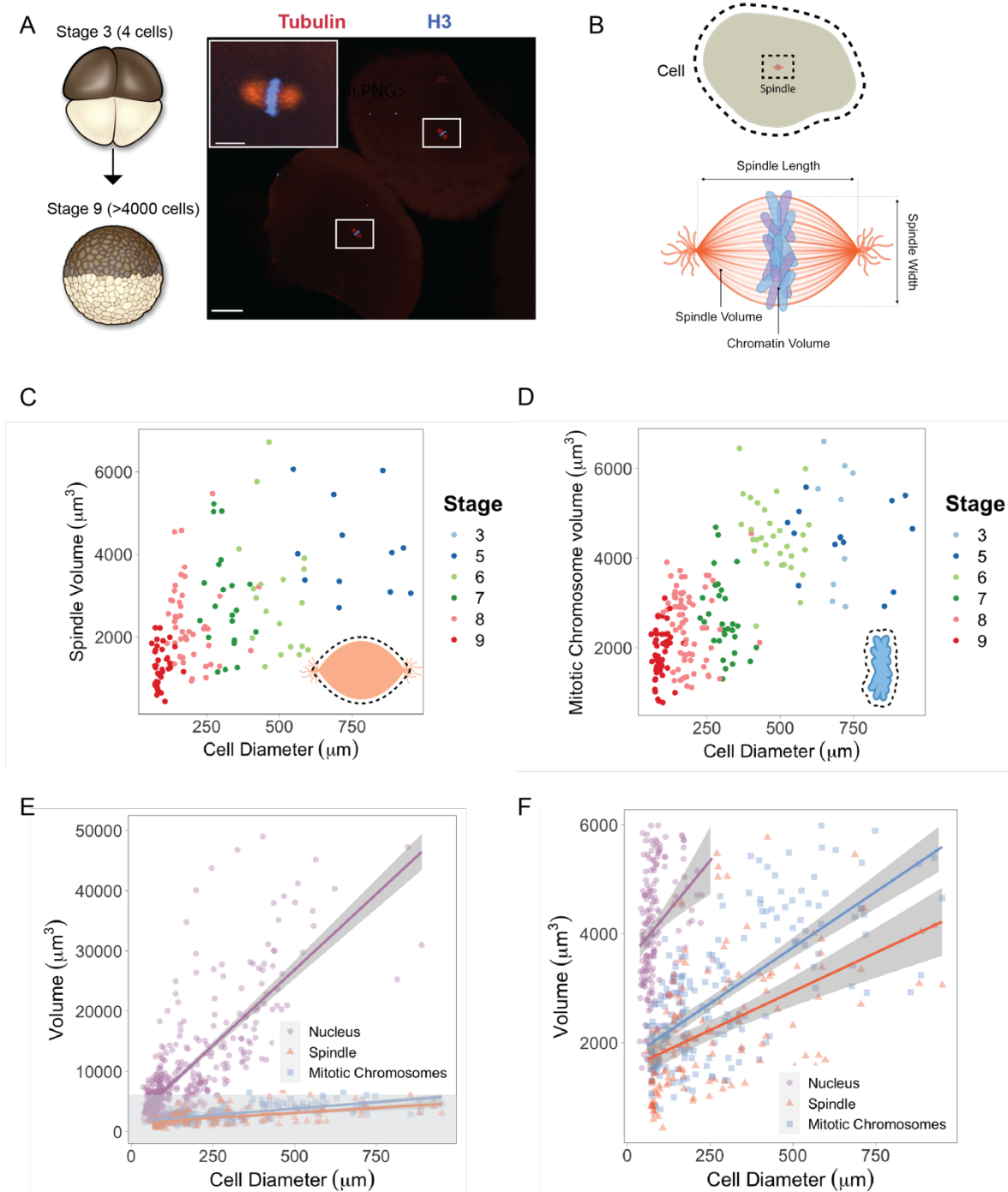
120   **Figure 1: Mitotic chromosomes scale continuously with cell size.** (A) Experimental scheme for whole-embryo immunofluorescence. Blastula-stage embryos were fixed during mitosis and stained with anti-histone H3 and anti-
121   tubulin antibodies to visualize mitotic chromosomes and spindles, respectively. Representative image of two cells
122   from a stage 6 embryo with white rectangles outlining mitotic spindles, scale bar = 100 µm. Inset: Magnified view
123   of one of the mitotic spindles, scale bar = 20 µm. (B) Dimensions of cells and spindles were either directly measured
124   or calculated (for details see Materials and Methods). (C) Measurements of spindle volume or (D) mitotic chromosome volume plotted against cell diameter, colored by developmental stage. (E) Volumes of spindles, nuclei and mitotic chromosomes all plotted against cell diameter, fit with linear models. 95% confidence intervals shown in gray. (F) Zoom-in of gray panel shown in (E). n = 2 biological replicates.

125
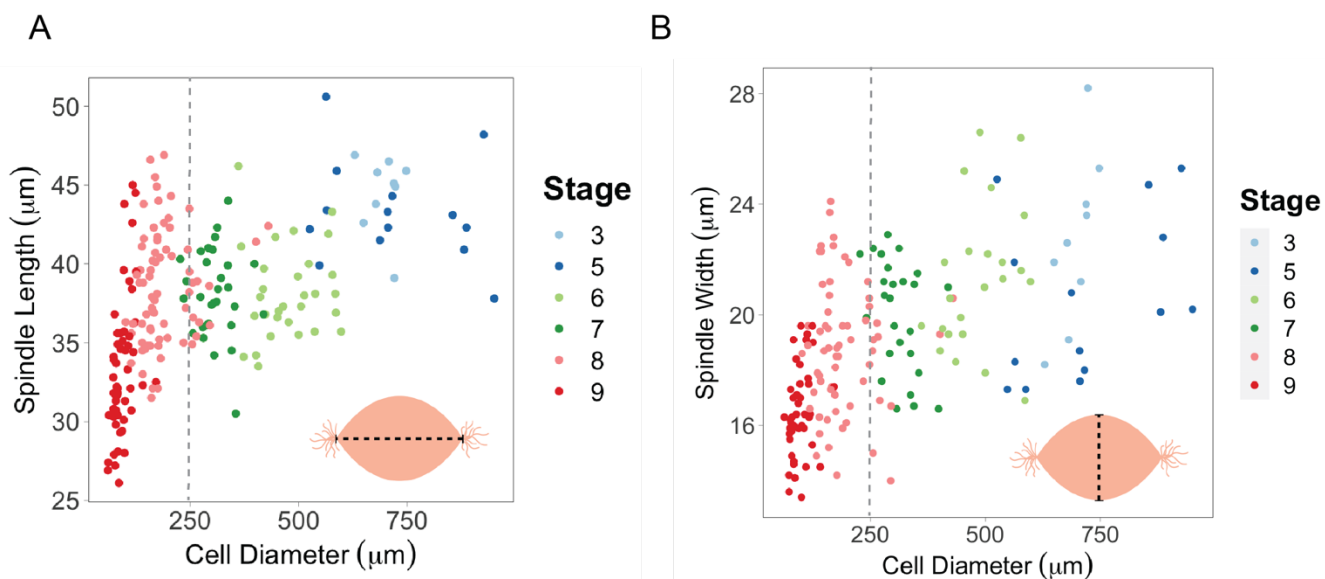
126
127 ***Figure 1, Supplement 1****: **Spindle lengths or widths vs. cell size.*** (A) Spindle lengths and (B) widths
128 plotted against cell diameter. Gray dotted lines show that spindle lengths plateau at around 250 μm while
129 spindle widths continue to increase.
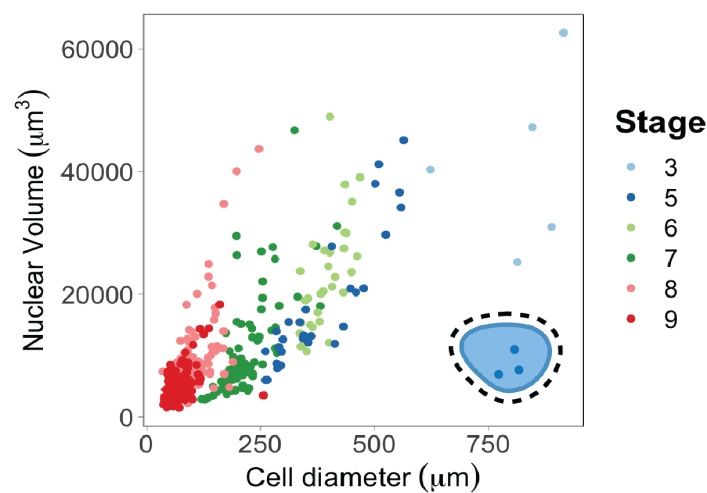130
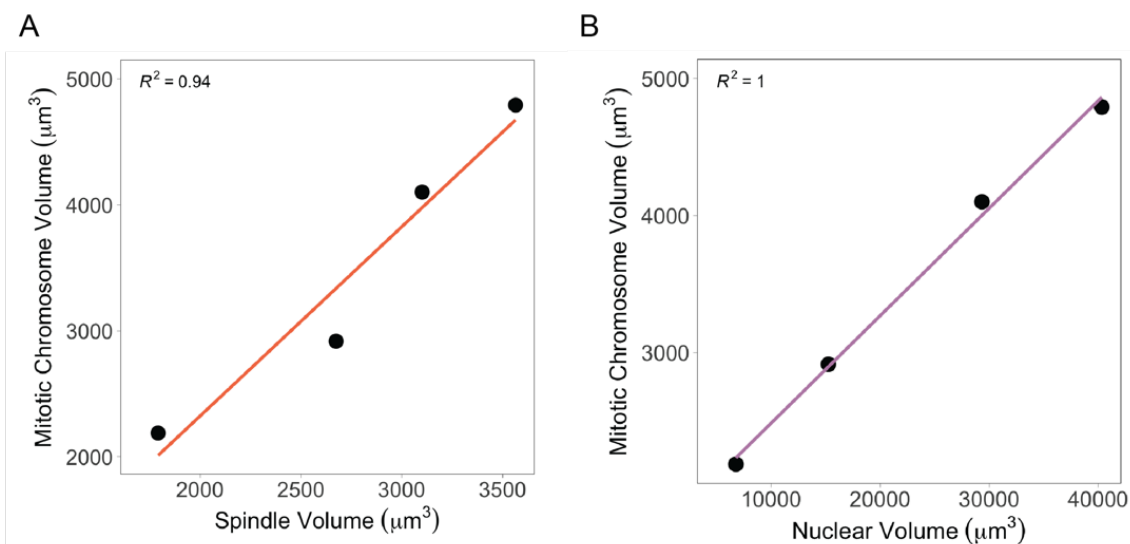131
132
133
134
135
136
137
138
139
140
141
142
143
144
145
146
147
148 ***Figure 1, Supplement 2: Nuclear volumes scale continuously with cell size.*** Nuclear volumes plotted
149 against cell diameter. Raw data used with permission from Jevtić and Levy, *Current Biology* 2015.
150
151
152
153
154
155
156
157
158

7

159 **Figure 1, Supplement 3: Mitotic chromosomes scale linearly with both nuclei and spindles.** (A)
160 Average mitotic chromosomes volumes plotted against (A) spindle volumes or (B) nuclear volumes, binned
161 by cell diameter (bin 1 = 35.1 – 219 μm, bin 2 = 219 – 402 μm, bin 3 = 402 – 585 μm, bin 4 = 585-768 μm).
162
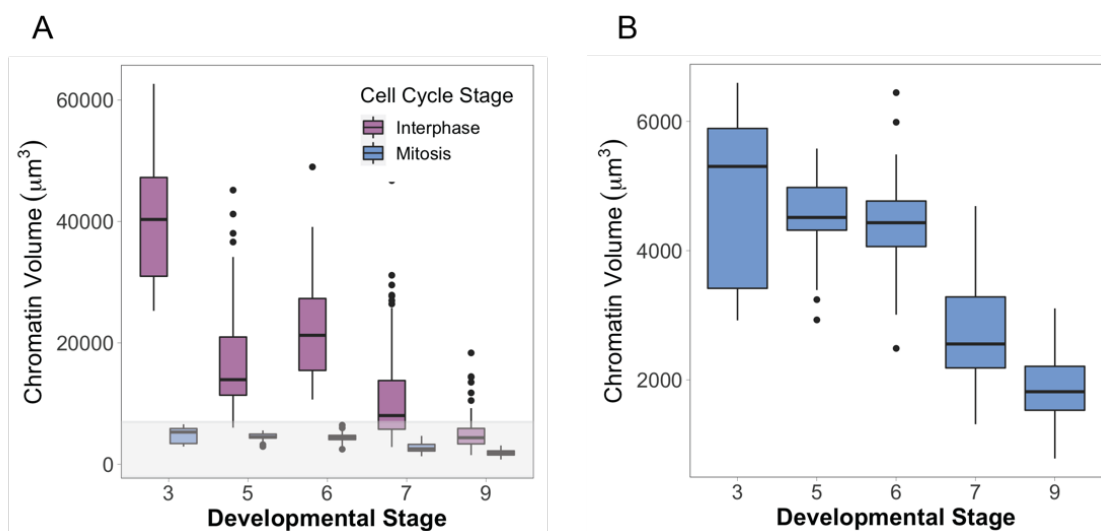
163
164 **Figure 1, Supplement 4: Nuclear vs. mitotic chromatin volumes during early cleavage divisions.** (A)
165 Chromatin volumes, either in interphase (purple) or metaphase (blue), binned by developmental stage. (B)
166 Zoomed-in view of data shown in the gray panel in (A), only for mitotic chromosomes.
167

168   **Mitotic chromosomes scale length-wise.**

169   To examine how morphologies of individual mitotic chromosomes change during development,

170   we prepared mitotic cell extracts from stage 3 (4-cell) or stage 8 (~4000-cell) embryos (Wilbur

171   and Heald, 2013) and centrifuged single endogenous mitotic chromosomes onto coverslips for

172   size measurements. We found that median chromosome lengths decreased ~2-fold between

173   stage 3 and stage 8 (Figure 2A-B), similar to the magnitude of mitotic chromosome scaling during

174   this period estimated by whole-embryo immunofluorescence (~2-3-fold, Figure 1D) and indicating

175   that shortening of the long axis is the predominant metric underlying mitotic chromosome scaling

176   during early embryogenesis. We also observed that the median length of endogenous stage 3

177   mitotic chromosomes was not statistically different from that of replicated sperm chromosomes

178   formed in egg extracts (Figure 2B), demonstrating that replicated sperm chromosomes formed in

179   egg extracts serve as a proxy for mitotic chromosome size during the earliest cell divisions.

180

181   Previously, it was shown that mixing mitotic extracts prepared from early and late blastula stage

182   embryos resulted in spindles of intermediate size due to equilibration of cytoplasmic spindle

183   scaling factors (Wilbur and Heald, 2013). Likewise, combining interphase extracts at different

184   ratios from two *Xenopus* species with different sized nuclei produced a graded effect on nuclear

185   size (Levy and Heald, 2010). To test whether a similar mechanism operates on mitotic

186   chromosomes, we combined metaphase-arrested egg extracts in a 1:1 ratio with stage 8 mitotic

187   embryo extracts containing endogenous mitotic chromosomes (Figure 2B). However, we

188   observed no increase in chromosome length, indicating that mitotic chromosome scaling factors

189   are not exchangeable in the cytoplasm during metaphase. To test whether mitotic chromosome

190   scaling could occur if initiated before the onset of chromosome condensation, we filtered stage 8

191   extracts to remove endogenous chromosomes and added back unreplicated sperm

192   chromosomes or sperm nuclei that had undergone replication in egg extracts (Figure 2C). In both

193   cases, sperm chromosomes were at least 2-fold longer than the endogenous stage 8

194   chromosomes (Figure 2D). Thus, mitotic chromosome size is predominantly set by factors loaded

195   during interphase that are not exchangeable, making mitotic chromosome scaling fundamentally

196   distinct from nuclear or spindle size scaling.
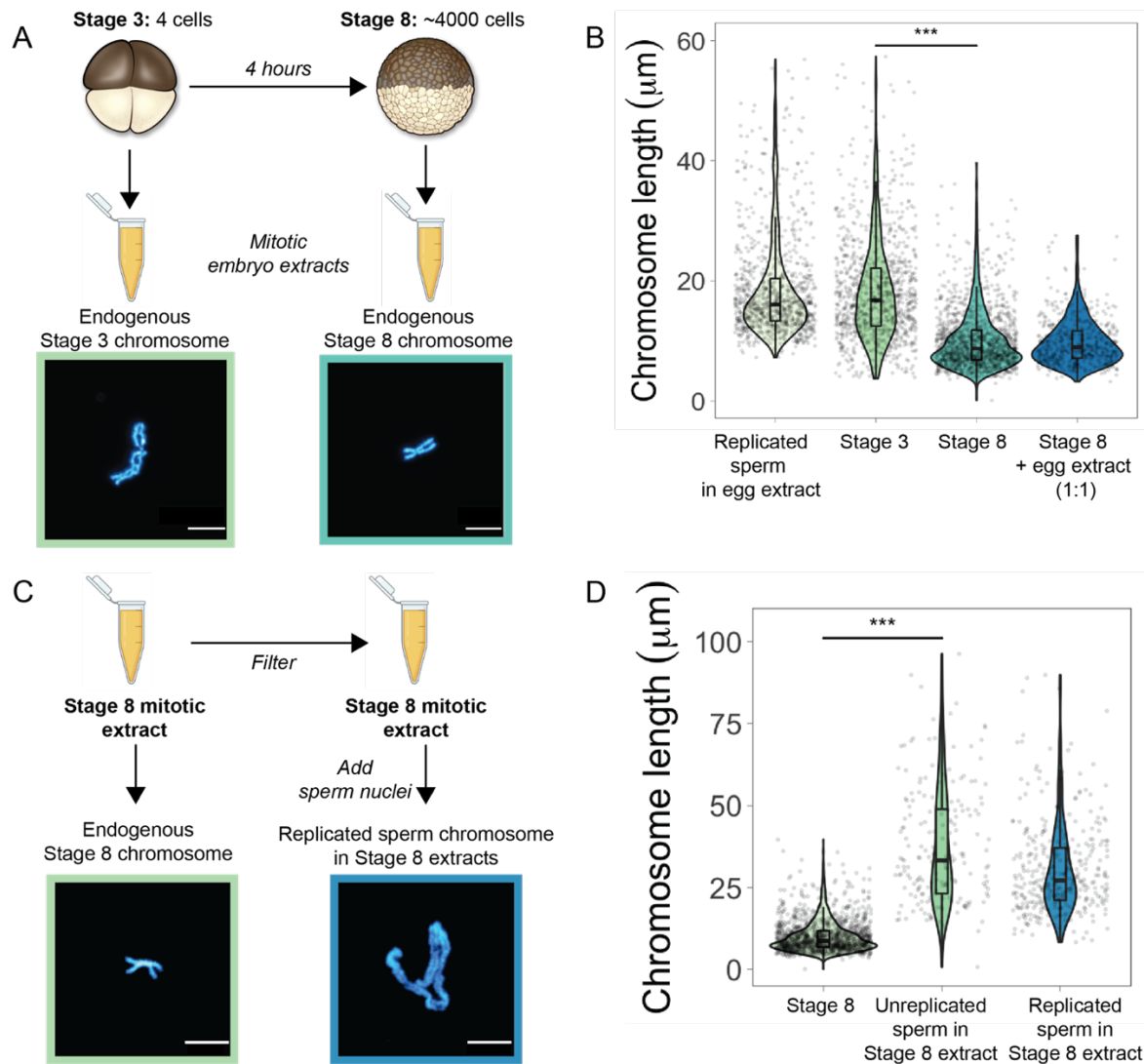
197

198   **Figure 2: Mitotic chromosomes scale length-wise.** (A) Mitotic extracts were prepared from stage 3 or
199   stage 8 embryos and endogenous, individual mitotic chromosomes were centrifuged onto coverslips and
200   stained with Hoechst DNA dye. Representative images of stage 3 and stage 8 chromosomes are shown.
201   (B) Length distributions of sperm mitotic chromosomes replicated in egg extract, mitotic chromosomes
202   isolated from embryo extracts and stage 8 embryo extract chromosomes after mixing 1:1 with egg extract.
203   (C) Stage 8 extracts were filtered to remove endogenous chromosomes, then unreplicated or replicated
204   sperm nuclei were added to form mitotic chromosomes. Representative images of endogenous stage 8
205   chromosome or replicated sperm chromosome formed in stage 8 extracts shown here. (D) Quantification
206   of chromosome lengths for the experiment shown in (C). n=3 biological replicates, >50 chromosomes per
207   replicate. Scale bar = 10 μm. *** denotes $p < 0.001$ by one-way ANOVA statistical testing.

208
209

210 **Mitotic chromosome size is determined by nuclear factors during interphase.**

211 The results above indicated that mitotic chromosome size is largely determined by nuclear rather

212 than cytoplasmic factors. Consistent with this idea, we confirmed previous results that G2-

213 arrested nuclei from blastula-stage embryos added to metaphase egg extracts produced mitotic

214 chromosomes ~2-fold shorter than replicated sperm chromosomes formed in the same extract

215 (Figure 3A, C; (Kieserman and Heald, 2014)). This finding suggested that mitotic chromosome

216 size is determined prior to entry into metaphase, likely by chromatin factors loaded during

217 interphase. The 2-fold difference in chromosome size was also recapitulated in extracts depleted

218 of membranes through ultracentrifugation, which are unable to form spindles but are competent

219 for mitotic chromosome assembly, indicating that spindle formation is not required for mitotic

220 chromosome scaling (Figure 3-S1). Previous work in *C. elegans* suggested that mitotic

221 chromosome size correlates with intranuclear density and nuclear size (Hara et al., 2013), but we

222 observed that embryo nuclei were larger than interphase sperm nuclei, and mitotic spindles

223 formed in egg extracts with these two sources of nuclei were indistinguishable in size (Figure 3-

224 S2). These data further suggest that scaling of spindles, nuclei and mitotic spindles are not

225 necessarily coordinated.

226

227 Interestingly, although mitotic chromosome scaling could be recapitulated by adding embryo

228 nuclei to metaphase-arrested egg extracts, chromosome morphologies were distinct. The

229 separation of sister chromatid arms resulting in X-shaped mitotic chromosomes in both stage 3

230 and stage 8 mitotic embryo extracts (Figure 2A) was not observed when stage 8 embryo nuclei

231 were added to egg extracts, as chromosome arms remained tightly associated along their lengths

232 (Figure 3B). Taken together, these results indicate that factors determining mitotic chromosome

233 size remain associated with G2-arrested embryo nuclei when placed into metaphase egg extracts,

234 while factors required for regulating sister chromatid arm cohesion do not.

235

Chromosome scaling correlates with differential recruitment of condensin I, topo II, and histone H1.8.

Robust recapitulation of chromosome scaling in metaphase-arrested egg extracts enabled molecular-level analysis of potential scaling factors, which was not technically feasible in embryo extracts that cannot transit the cell cycle *in vitro*. We examined three proteins known to influence chromosome size and morphology in *Xenopus*, condensin I (the predominant condensin in *Xenopus* eggs), topoisomerase II (topo II), and the maternal linker histone, termed H1.8 (Maresca et al., 2005; Nielsen et al., 2020; Shintomi and Hirano, 2011). After performing immunostaining of short embryo chromosomes or long sperm chromosomes formed in the same egg extracts, the abundance of each factor was calculated by normalizing immunofluorescence signal to DNA dye intensity (Figure 3B, see Materials and Methods). We found that short embryo chromosomes contained less condensin I and topo II, but more H1.8 relative to long replicated sperm chromosomes (Figure 3D). These results are consistent with studies showing that depletion of H1.8 from egg extracts lengthens mitotic chromosomes (Maresca et al., 2005). Furthermore, it was recently shown that H1.8 inhibits binding of condensin I and topo II to mitotic chromosomes (Choppakatla et al., 2021). Therefore, differential recruitment of condensin, topo II, or H1.8 may contribute to mitotic chromosome scaling during embryogenesis.

Our previous work showed that short embryo chromosomes could be reset to lengths observed in replicated sperm samples by cycling the mitotic chromosomes through an additional interphase in egg extracts (Figure 3-S3A; (Kieserman and Heald, 2014)). To test whether the abundance of candidate scaling factors was affected, we performed immunofluorescence on mitotic embryo chromosomes before and after the additional interphase. We found that the abundance of all three factors on mitotic chromosomes increased on the embryo chromosomes (Figure 3-SC-F), which also doubled in length (Figure 3-S3B). Of the three factors, condensin I levels increased the most (2-fold), returning to levels found on replicated sperm chromosomes (Figure 3-S3C). Our

12

262   observation that H1.8 levels increased slightly after the second metaphase suggests that

263   condensin I abundance is not necessarily regulated by H1.8, and that condensin I can override

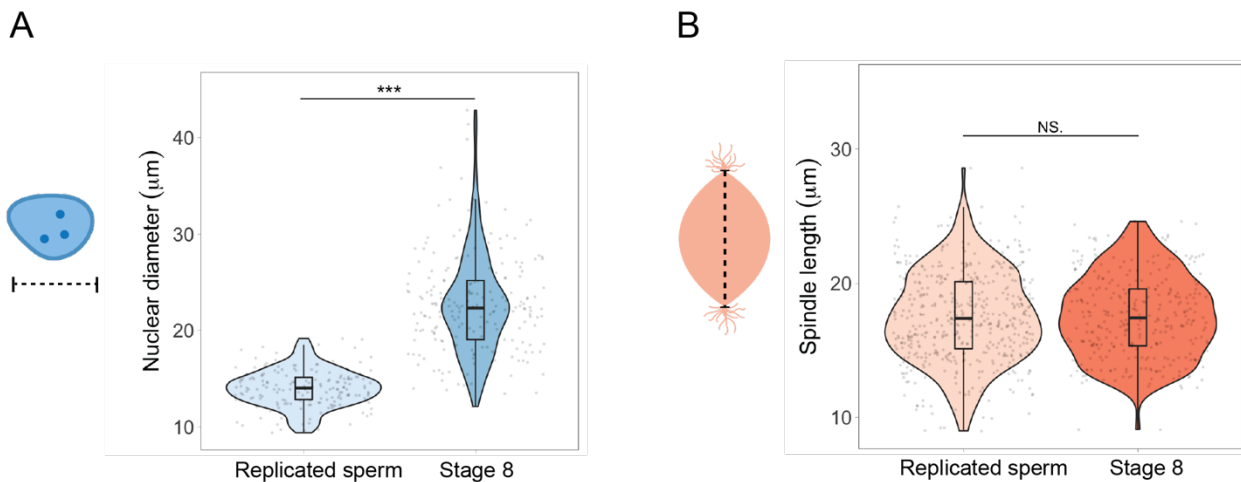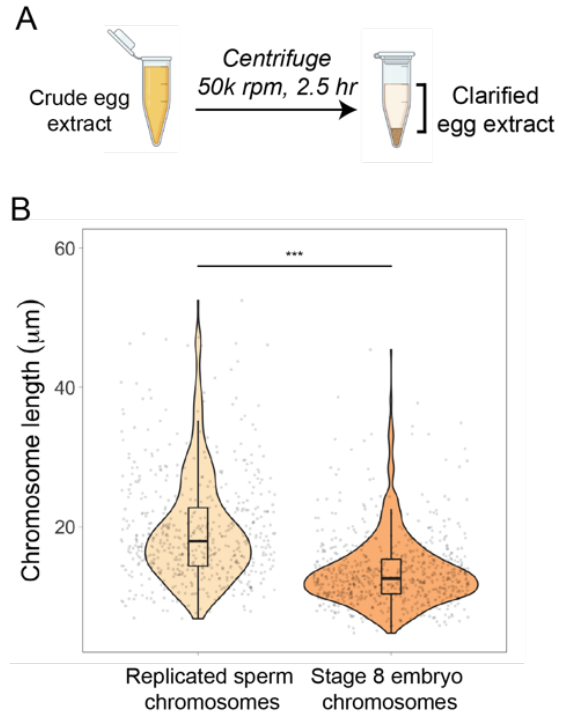264   the condensation activity of H1 to lengthen embryo chromosomes.

265
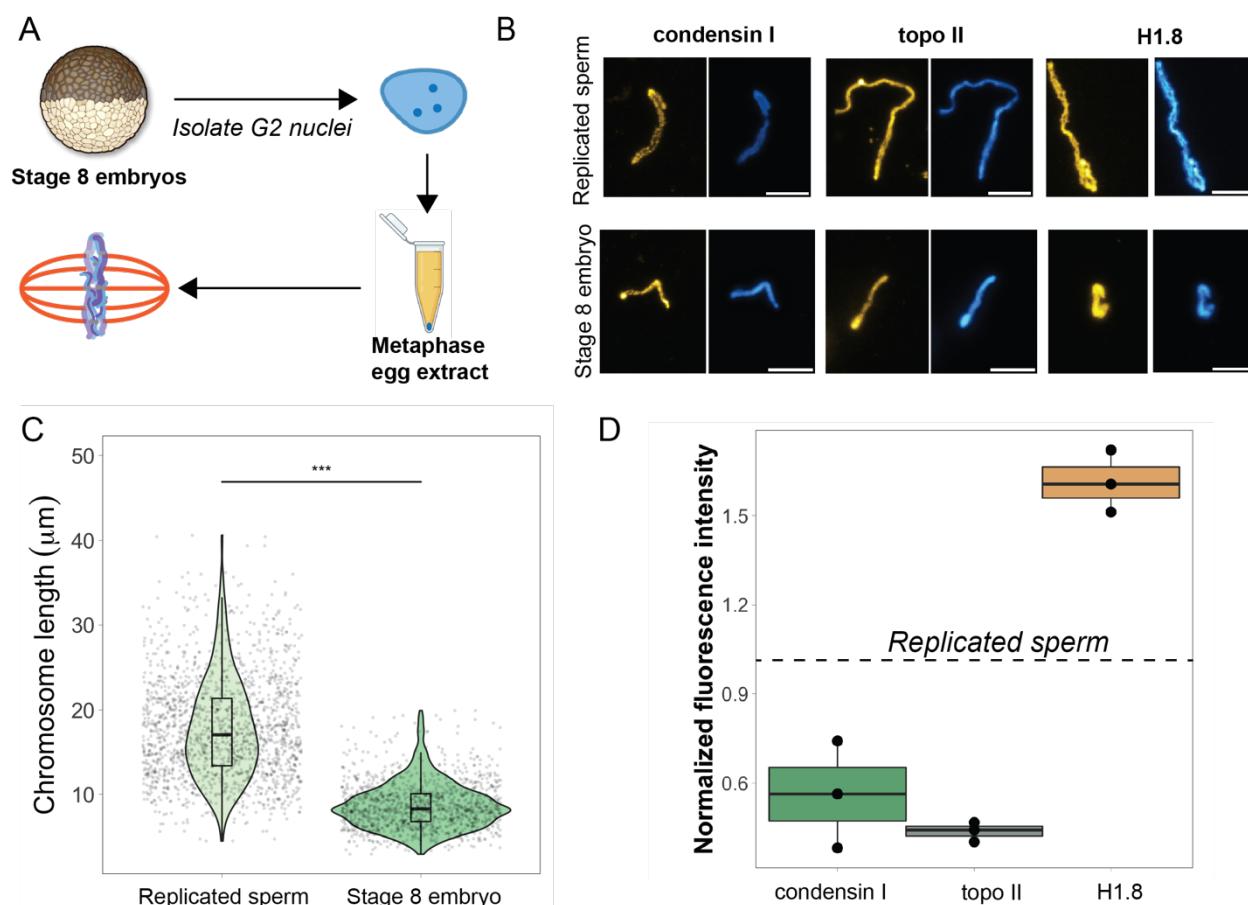
266

267   **Figure 3: Egg extracts recapitulate mitotic chromosome scaling through differential recruitment of**
268   **condensin I, topo II, and histone H1.8.** (A) Experimental scheme. Stage 8 embryos arrested in G2 with
269   cycloheximide were used to prepare extracts, then embryo nuclei were pelleted and added to metaphase-
270   arrested egg extracts to form mitotic spindles and chromosomes. (B) Representative images of mitotic
271   chromosomes prepared by adding replicated sperm nuclei (top) or stage 8 embryo nuclei (bottom) to
272   metaphase egg extracts, and stained with antibodies for condensin I, topo II or H1.8. Scale bar = 10 µm.
273   (C) Lengths of replicated sperm chromosomes or stage 8 embryo chromosomes formed in metaphase egg
274   extracts. n>3 biological replicates, >50 chromosomes per replicate. *** denotes $p < 0.001$ by one-way
275   ANOVA statistical testing. (D) Abundances of topo II, condensin I and H1.8 (calculated by normalizing
276   immunofluorescence signal to Hoechst signal, see Materials and Methods for details) on short embryo
277   chromosomes normalized to long sperm chromosomes (shown by dotted line), from three different extracts.
278

279

280 ***Figure 3, Supplement 1: Clarified egg extracts***
281 ***recapitulate mitotic chromosome scaling.*** (A)
282 Crude extracts were centrifuged at high speed to pellet
283 membranes. (B) Quantification of mitotic chromosome
284 lengths from either replicated sperm nuclei or stage 8
285 embryo nuclei added to clarified metaphase egg
286 extracts. n=3 biological replicates, >50 chromosomes
287 per replicate. *** denotes p <0.001 by one-way ANOVA
288 statistical testing.

289
290
291
292
293
294
295
296
297
298
299
300
301

302
303
304 ***Figure 3, Supplement 2: Nuclei and spindles do not scale with mitotic chromosome size in egg***
305 ***extracts.*** (A) Diameters of replicated sperm nuclei or stage 8 embryo nuclei just before placing into
306 metaphase egg extracts. (B) Lengths of spindles formed around either replicated sperm nuclei or embryo
307 nuclei in metaphase egg extracts. n=3 biological replicates, >50 structures per replicate. *** denotes p
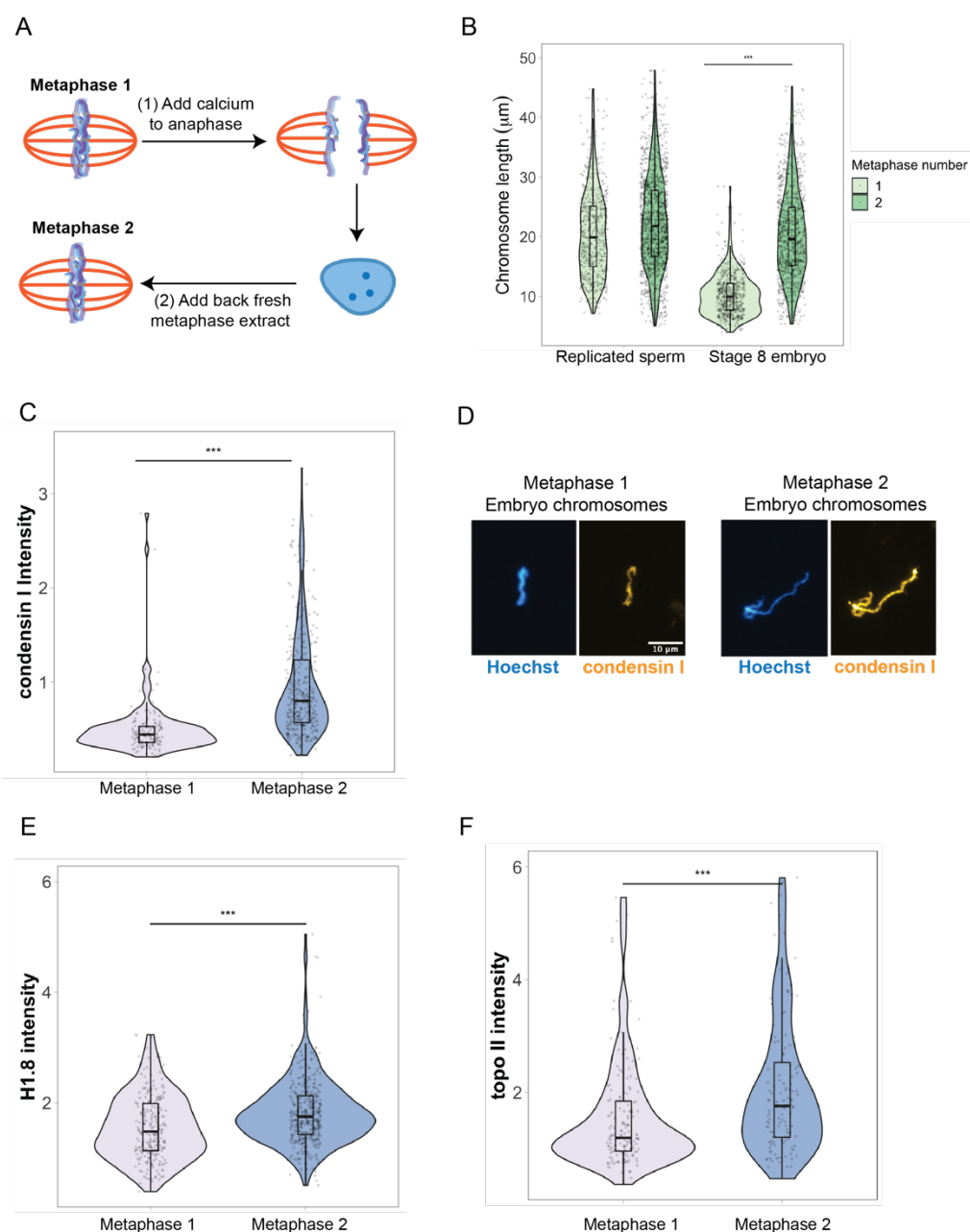308 <0.001 by one-way ANOVA statistical testing.

14

Figure 3, Supplement 3: Scaling factors are re-loaded onto embryo chromosomes after an additional interphase in egg extracts. (A) Schematic of anaphase experiment. Calcium is added to send metaphase spindles containing embryo chromosomes into anaphase, and then interphase. After nuclei formed, fresh metaphase extract was added to trigger mitotic chromosome formation. (B) Quantification of chromosome lengths for the first and second metaphase comparing replicated sperm and stage 8 embryo mitotic chromosomes. (C) Abundance of condensin I on stage 8 embryo chromosomes in the first or second metaphase. (D) Representative images of embryo chromosomes from metaphase 1 or metaphase 2, stained for condensin I. (E-F) Abundance of H1.8 and topo II on stage 8 embryo chromosomes in the first or second metaphase. Based on median values, condensin I increased 2-fold, H1.8 increased 1.2-fold and topo II increased 1.5 fold from the first to second metaphase. n=3 biological replicates, >50 chromosomes per replicate. *** denotes p <0.001 by one-way ANOVA statistical testing.

15

365 **Mitotic chromosomes scale through extensive remodeling of DNA loop architecture.**

366 Condensin shapes mitotic chromosomes through its ability to form and extrude loops from the

367 central axis (Ganji et al., 2018; Goloborodko et al., 2016). *In silico* models of loop extrusion activity

368 suggested that tuning the abundance of condensin could dramatically alter DNA loop architecture

369 and thus chromosome dimensions (Goloborodko et al., 2016). However, these models have not

370 been tested under physiological conditions that relate to chromosome size changes *in vivo*.

371

372 To assess how DNA loop size and arrangement is altered in the context of mitotic chromosome

373 scaling, we performed Hi-C on long sperm chromosomes and short embryo chromosomes formed

374 in egg extracts. Hi-C contact maps indicate that short embryo chromosomes had increased

375 genomic contacts along their entire length, as evidenced by thickening of the diagonal (Figure

376 4A). To quantify this effect, we plotted the decay of contact frequencies *(P)* as a function of

377 genomic distance in bp (*s*) (Figure 4B). We find that the shape of $P(s)$ is similar to what we

378 observed in earlier work for mitotic chromosomes from human, chicken and *Xenopus*

379 (Choppakatla et al., 2021; Gibcus et al., 2018; Naumova et al., 2013), and for rod-shaped

380 dinoflagellate chromosomes (Nand et al., 2021). $P(s)$ is characterized by two regimes: an initial

381 regime where the slope is rather small, followed by a regime where the slope is much steeper.

382 We have shown that this shape is characteristic of compact rod-shaped chromosomes that are

383 organized in layers (Naumova et al., 2013), and the genomic distance where the slope suddenly

384 increases is related to the amount of DNA that is packed per layer. Loci within a layer often

385 interact, but loci separated by a genomic distance that is larger than the layer size rarely do

386 because of the stiffness of the chromosome. Within a layer, chromosomes are organized as loops,

387 the size of which can be estimated from the derivative of $P(s)$ (Johan H. Gibcus et al., 2018), the

388 loop size is around where the derivative displays a maximum (Figure 4C).

389

390   We find that $P(s)$ for short embryo chromosomes differ in two ways from long sperm

391   chromosomes. First the layer size is larger, i.e., ~10^7 bp vs. 10^6 bp (Figure 4C, gray bar), which

392   would be expected for shorter chromosomes where more DNA is packed within a cross-section

393   of a chromosome. Second, DNA loop size is considerably larger for short embryo chromosomes,

394   as is visible in a rightward shift in the peak of the derivative of $P(s)$ (Figure 4C, orange bar). This

395   analysis, combined with our immunofluorescence results from Figure 3, is consistent with a model

396   where mitotic chromosomes scale through decreased recruitment of condensin I, resulting in

397   larger DNA loops and more DNA per layer, thus accommodating more DNA on a shorter

398   chromosome axis (Figure 4D).

399
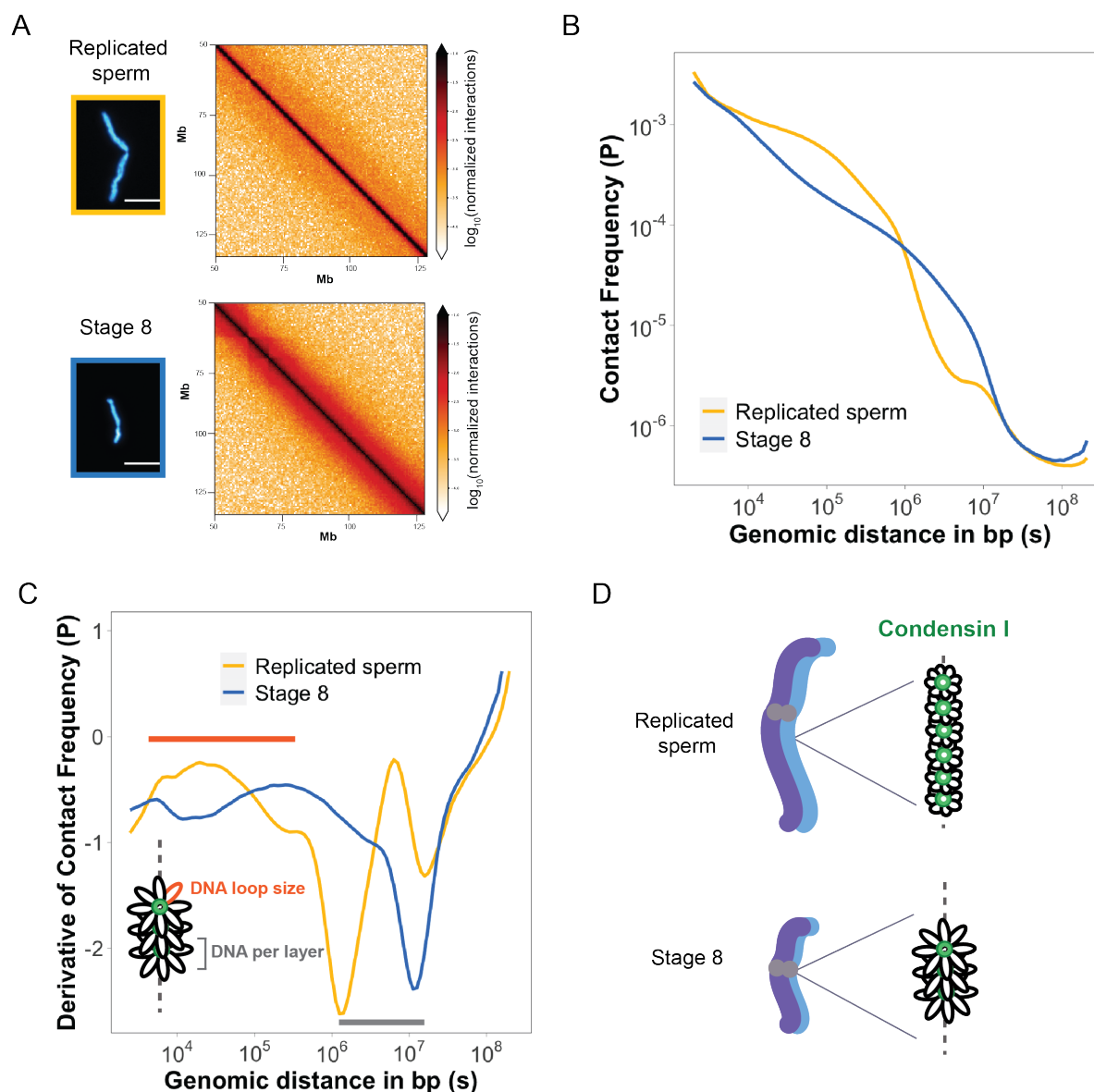
Figure 4: Mitotic chromosomes scale through extensive remodeling of DNA loop architecture. (A) Hi-C maps of chromosome 4S from replicated sperm or stage 8 embryo chromosomes formed in metaphase egg extracts. (B) Plots comparing how contact frequency *(P)* genome-wide decays as a function of genomic distance *(s)* for replicated sperm (yellow) or stage 8 mitotic chromosomes (blue). (C) Derivative of contact frequencies from (B). Based on previous models, the difference in inflection point at 10^4-10^6 bp represents a difference in loop size (orange), while the difference in inflection point at 10^6-10^7 bp represents a difference in DNA per layer (gray). (D) Model depicting how lower condensin I occupancy on short embryo chromosomes results in an increase in DNA loop size and DNA per layer. n= 2 biological replicates.

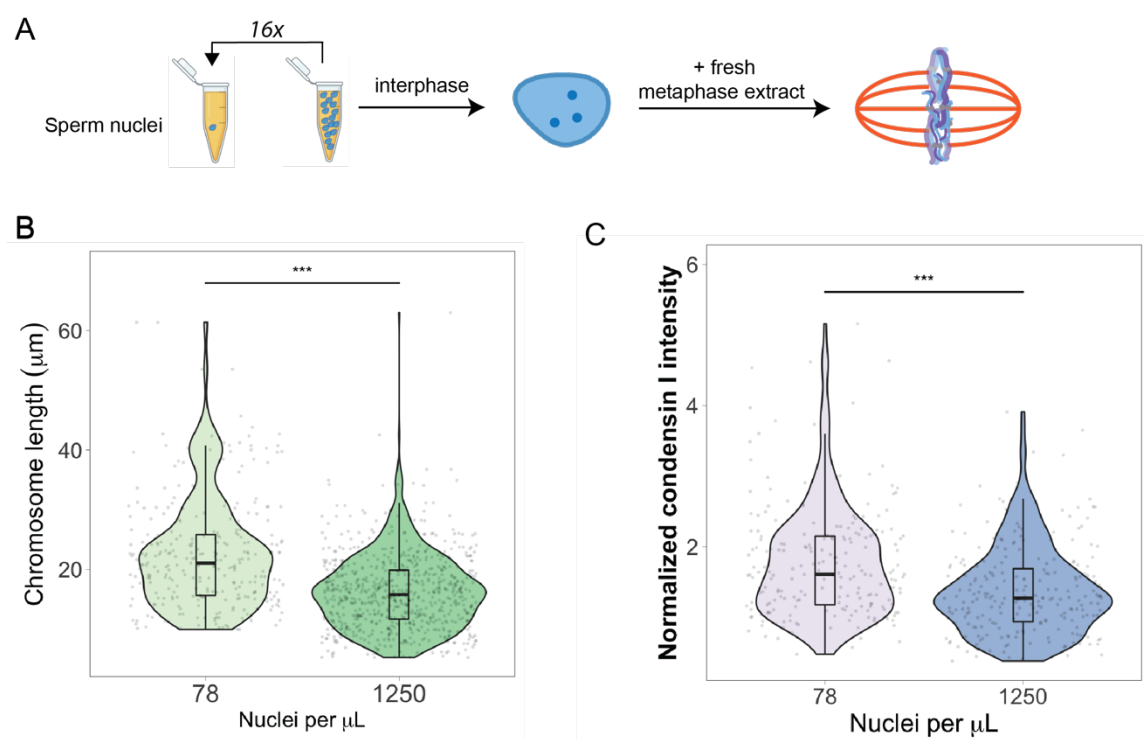**Nucleo-cytoplasmic ratio regulates mitotic chromosome scaling, but not nuclear or spindle scaling**

We next investigated the developmental cues that could decrease the abundance of condensin I on mitotic chromosomes as they scale during development. Characteristic features of cleavage divisions during early embryogenesis are the lack of cell growth and minimal gene expression, resulting in exponentially increasing copies of the genome within the same total volume and content of cytoplasm. The increase in nucleo-cytoplasmic (N/C) ratio, defined here as the number of nuclei per volume of cytoplasm, titrates a finite maternal pool of DNA binding factors that are distributed to more and more genomes over time, thus lowering their abundance per genome. This effect is thought to underlie activation of zygotic transcription at the mid-blastula transition (Amodeo et al., 2015), and titration of the histone chaperone Npm2 was shown to play a role in nuclear scaling (Chen et al., 2019).

To test whether N/C ratio could play a role in mitotic chromosome scaling, we varied the concentration of sperm nuclei at two different densities corresponding to early (~75 sperm nuclei/μl) and late (~1250 nuclei/μl) blastula stage embryos (Figure 5A). We first allowed these nuclei to replicate in interphase egg extracts, then added back fresh metaphase extracts before analyzing mitotic chromosome lengths and abundances of condensin I, topo II and H1.8. We found that increasing N/C ratio decreased mitotic chromosome size by ~1.5 fold (Figure 5B), consistent with the difference observed *in vivo* at the stages of development that correspond to the N/C ratios tested (Stage 6-7, Figure 1D). This 1.5-fold change in chromosome size also correlated with a 1.5-fold decrease in condensin I abundance on mitotic chromosomes (Figure 5C), and with less significant changes for H1.8 and topo II abundance (Figure 5-S1). Interestingly we found that increasing N/C ratio did not significantly affect nuclear size and actually led to an increase in spindle size (Figure 5-S2), suggesting that N/C ratio is only sufficient to scale mitotic chromosome size during embryogenesis.

436   To examine whether the titration effect of chromosome factors observed *in vitro*

437   corresponded to changes in their abundance during development *in vivo*, we measured levels of

438   condensin I, H3 and histone H1.8 on embryo nuclei isolated from different stages. As predicted,

439   although protein concentrations in embryos did not change over the course of the early cleavage

440   divisions (Figure 5-S3A), levels of all factors on interphase nuclei decreased as genome copy

441   number increased (Figure 5-S3B). Furthermore, adding different concentrations of stage 8

442   embryo nuclei to egg extracts did not significantly change mitotic chromosome size (Figure 5-S4),

443   consistent with the idea that titration of maternal factors had already occurred in the embryo, and

444   that interphase factors set chromosome size during metaphase. Together these observations

445   confirm that maternally loaded factors are titrated onto newly synthesized copies of the genome,

446   and that increasing N/C ratio is sufficient to shorten mitotic chromosomes, likely by decreasing

447   levels of condensin I.

448

449   **Figure 5: Nucleo-cytoplasmic ratio regulates mitotic chromosome scaling, but not nuclear or**
450   **spindle scaling.** (A) Concentration of sperm nuclei in egg extracts was varied 16-fold to mimic
451   concentrations found in early (78 nuclei/μL) vs. late (1250 nuclei/μL) blastula stages. (B) Quantification of

452   mitotic chromosome lengths and (C) condensin I intensities, normalized to Hoechst signal, in samples
453   containing high or low concentrations of sperm nuclei. n=3 biological replicates, >50 chromosomes per
454   replicate, *** denotes p <0.001 by one-way ANOVA statistical testing.
455
456
457
458

459
460
461
462
463
464
465
466
467
468
469
470
471
472
473
474
475
476
477
478
479
480
481
482
483
484
485
486
487

488   ***Figure 5, Supplement 1: topo II and H1.8 exhibit less of a titration effect than condensin I.***
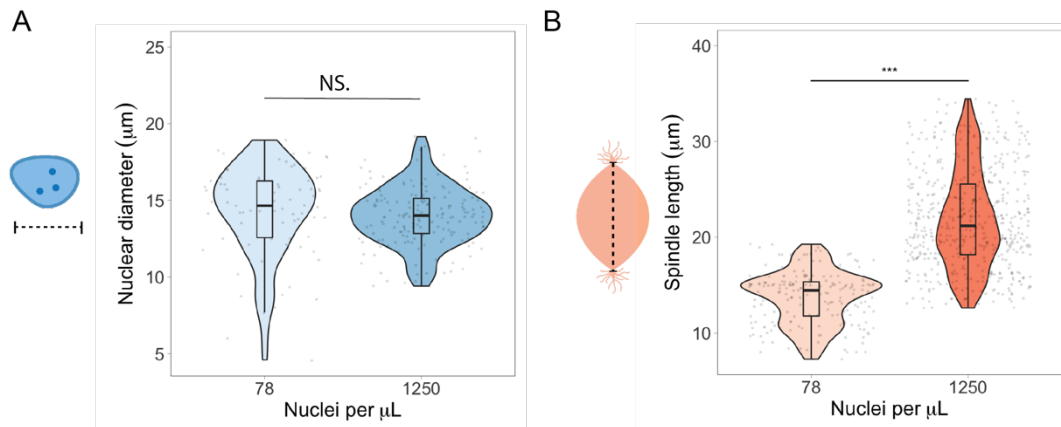489   Normalized fluorescence intensity of (A) H1.8, (B) topo II, and (C) H3 on sperm mitotic chromosomes in
490   samples containing low or high concentrations of nuclei. n=3 biological replicates, >50 chromosomes per
491   replicate, *** denotes p <0.001 by one-way ANOVA statistical testing.
492
493
494
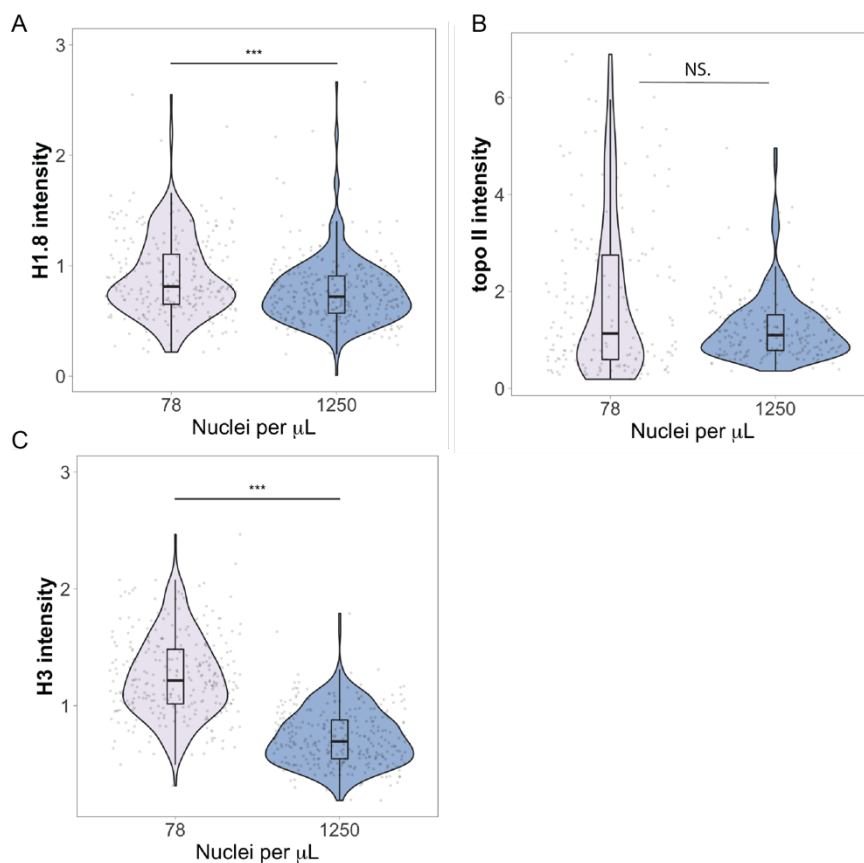
495
Figure 5, Supplement 2: N/C ratio does not regulate spindle or nuclear size. (A) Nuclear diameters plotted for samples containing low or high concentrations of sperm nuclei. (B) Spindle lengths plotted for samples containing low or high concentrations of sperm nuclei. n=3 biological replicates, >50 structures per replicate, *** denotes p <0.001 by one-way ANOVA statistical testing.
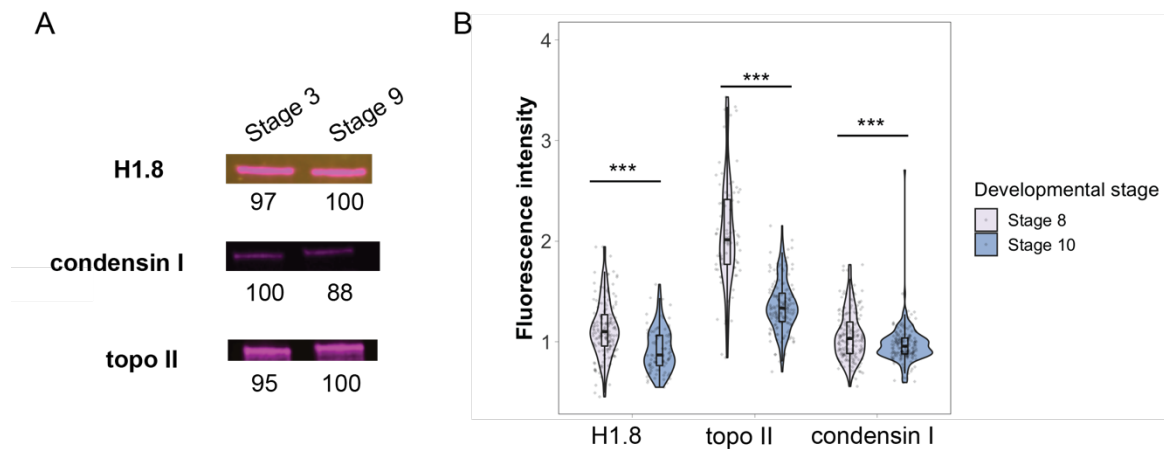
Figure 5, Supplement 3: Titration of nuclear factors during embryogenesis. (A) Western blots of whole embryo extracts from early (stage 3) or late (stage 9) blastula stages. Numbers below each band indicate the relative differences in signal intensity, normalized to the highest intensity band for that antibody. (A) Immunofluorescence of nuclei from stage 8 or 10 embryos showing the depletion of nuclear factors in later stages. n=3 biological replicates, >50 chromosomes per replicate, and *** denotes p <0.001 by one-way ANOVA statistical testing.
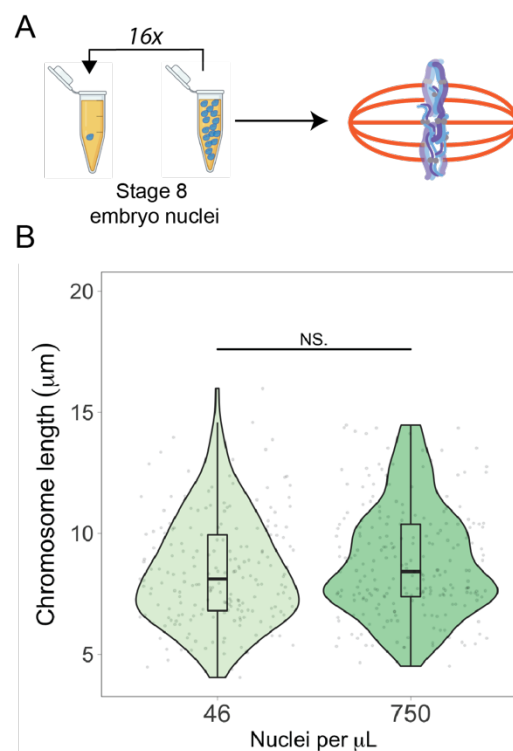
Figure 5, Supplement 4: Embryo mitotic chromosome lengths are not affected by nuclei density.
(A) Schematic of experiment. Stage 8 embryo nuclei were added to metaphase egg extracts at N/C ratios spanning a 16-fold range. (B) Quantification of mitotic chromosome lengths in samples containing high or low concentrations of stage 8 embryo nuclei. n=3 biological replicates, >50 chromosomes per replicate, and *** denotes p <0.001 by one-way ANOVA statistical testing.

554 **Importin α partitioning scales mitotic chromosomes to spindle and cell size.**

555 A major developmental cue central to the scaling of nuclei and spindles is cell size. We previously

556 identified importin α as a factor that coordinately scales nuclei and spindles to cell size by

557 regulating nuclear import of lamin proteins and the activity of a microtubule destabilizing protein,

558 respectively (Brownlee and Heald, 2019; Levy and Heald, 2010; Wilbur and Heald, 2013).

559 Palmitoylation of importin α drives a subset of the total population to the cell membrane, where it

560 can no longer interact with its nuclear localization sequence (NLS)-containing cargo that scale

561 mitotic spindles (Figure 6A). As cell size decreases during early cleavage divisions, cell surface

562 area/volume (SA/V) increases, causing more importin α to be driven to the membrane and more

563 scaling factors to be released into the cytoplasm (Figure 6A; (Brownlee and Heald, 2019)). To

564 address whether importin α also plays a role in mitotic chromosome scaling, we treated egg

565 extracts with palmostatin, an inhibitor of the major depalmitoylation enzyme APT1 to increase the

566 pool of palmitoylated importin α, thus mimicking smaller cells with higher cell SA/V (Figure 6B;

567 (Dekker et al., 2010)). We found that mitotic chromosome size decreased with palmostatin

568 treatment and was fully rescued by the addition of recombinantly purified importin α that cannot

569 be palmitoylatated (NP importin α), but not by addition of wild-type (WT) importin α (Figure 6B-

570 C). Surprisingly, we found no significant difference in condensin I abundance on mitotic

571 chromosomes formed in either DMSO or palmostatin-treated extracts (Figure 6D), suggesting

572 that importin α partitioning acts separately from the N/C pathway to scale mitotic chromosomes.

573 To determine when in the cell cycle palmostatin was affecting importin α cargos, we added it to

574 extracts either before interphase or following entry into metaphase (Figure 6E). Interestingly,

575 analogous to effects on spindle size but not nuclear size (Brownlee and Heald, 2019), we found

576 that palmostatin treatment during metaphase was sufficient to scale mitotic chromosomes (Figure

577 6F). Together these results demonstrate that partitioning of importin α during metaphase scales

578 mitotic chromosomes to spindle and cell size in a condensin I-independent pathway.
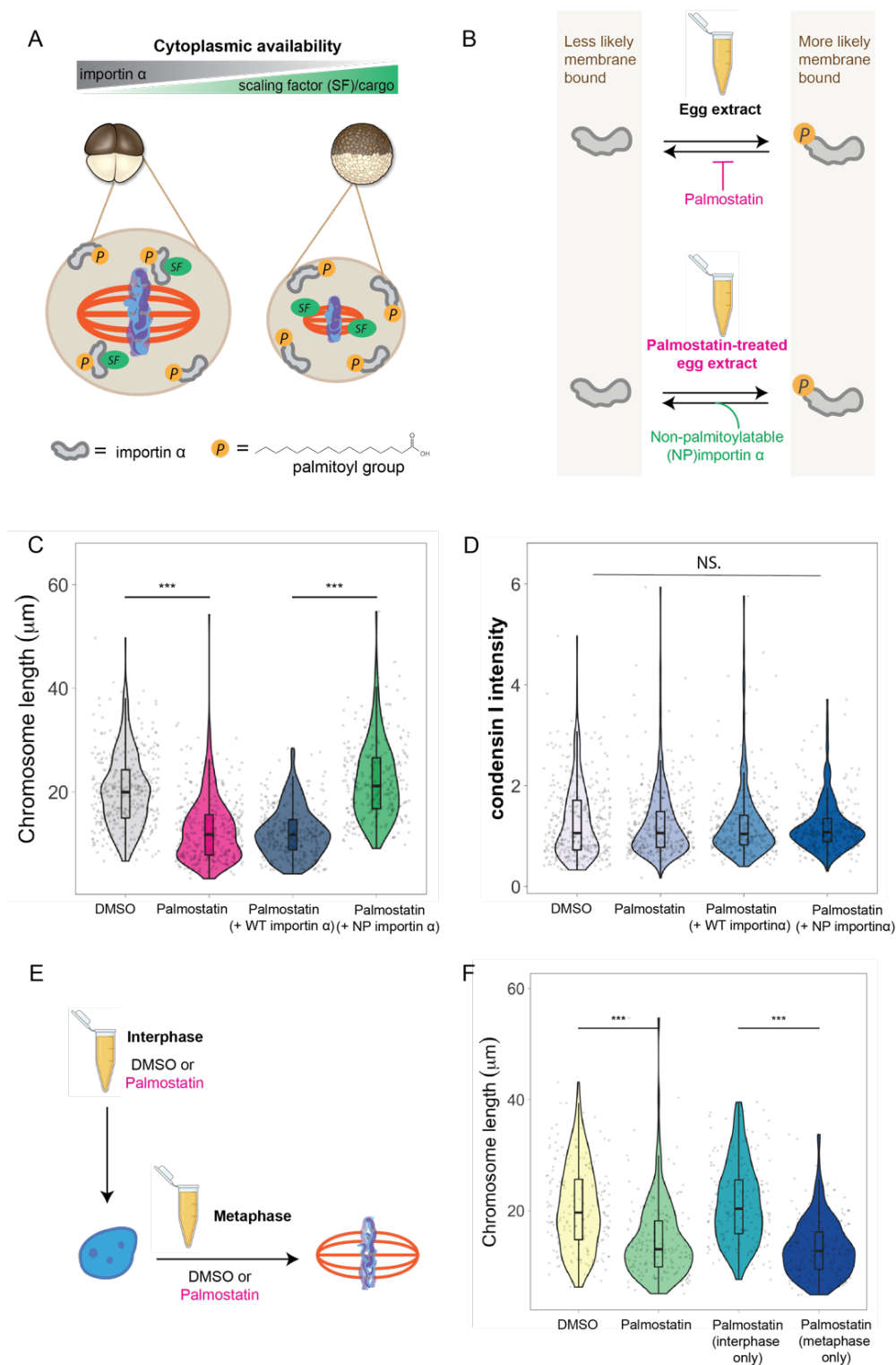
Figure 6: Importin α partitioning scales mitotic chromosomes to spindle and cell size. (A) Model for how importin α scales mitotic spindles to cell size. Due to palmitoylation of importin α, a portion of it is driven to the cell membrane, where it can no longer interact with nuclear localization sequence (NLS)-containing scaling factors, freeing them to shrink the mitotic spindle. As cell surface area/volume (SA/V) increases during embryogenesis, proportionally more importin α is driven to the membrane, thus increasing

635 the cytoplasmic availability of scaling factors. (B) Top, Inhibition of the major depalmitoylation enzyme APT1
636 in egg extracts mimics smaller cells by increasing the proportion of palmitoylated, membrane-bound
637 importin α. Bottom, addition of non-palmitoylatable (NP) importin α should rescue chromosome size in
638 palmostatin-treated egg extracts by increasing the proportion of cytoplasmic importin α. (C) Quantification
639 of mitotic chromosome lengths in palmostatin-treated extracts and rescue of chromosome length by
640 addition of non-palmitoylatable (NP) importin α but not by wild-type (WT) importin α. (D) Quantification of
641 condensin I intensity for the samples shown in (C). (E) Schematic of experiment to test whether importin α
642 partitioning plays a role in chromosome scaling during interphase or metaphase. (F) Quantification of
643 chromosome lengths for experiment described in (E). n=3 biological replicates, >50 chromosomes per
644 replicate, and *** denotes p <0.001 by one-way ANOVA statistical testing.

645
646

647 **Discussion**

648 The results described here provide a comprehensive view of how mitotic chromosome size is

649 regulated by different developmental cues during early cleavage divisions of *Xenopus* embryos.

650 Our data suggest that mitotic chromosomes coordinately scale with spindle and cell size through

651 importin α partitioning. Additionally, increasing N/C ratio is sufficient to scale mitotic chromosomes

652 through decreased recruitment of condensin I, resulting in increased DNA loop and layer size and

653 length-wise compaction. As detailed below, our findings have important implications for the

654 interplay between subcellular scaling and chromosome structure during early embryogenesis.

655

656 <u>Mitotic chromosome size is not necessarily coupled to nuclear and spindle size</u>. Previous work in

657 *C. elegans* showed that mitotic chromosome size correlated positively with nuclear size and

658 negatively with intranuclear density (Hara et al., 2013; Ladouceur et al., 2015). However, in egg

659 extracts, mitotic chromosome size does not necessarily correlate with spindle and nuclear size.

660 G2-arrested stage 8 embryo nuclei, which contain both the maternal and paternal genomes, are

661 almost 2-fold larger than replicated sperm nuclei (Figure 3-S2A), consistent with a 2-fold increase

662 in genome content. Yet when added to metaphase egg extracts, they form mitotic chromosomes

663 that are 2-fold shorter than replicated sperm chromosomes (Figure 3C), demonstrating that mitotic

664 chromosomes don't necessarily scale to either intranuclear density or nuclear size. We also

665 showed that though mitotic chromosomes scale continuously with spindle size *in vivo* (Figure 1),

666 this correlation is abolished *in vitro* (Figure 3-S2B). In a completely different set of experiments,

667 when N/C ratio was varied in egg extracts (Figure 5), mitotic chromosomes shrank 1.5-fold while

668 spindle size increased almost 2-fold and nuclear size remained constant. Together these data

669 suggest that the mechanisms that regulate the size of mitotic chromosomes, spindles and nuclei

670 are distinct.

671

672 <u>Mitotic chromosome scaling involves temporally and spatially distinct developmental cues.</u>

673 Whereas mitotic spindle size and nuclear size are set by factors operating during metaphase and

674 interphase, respectively, we found that both phases of the cell cycle contribute to scale mitotic

675 chromosomes. Our embryo extract and egg extract data (Figures 2 and 3) suggest that mitotic

676 chromosome size is determined by factors already present in interphase nuclei and cannot be re-

677 set by metaphase egg extracts. On the other hand, importin α partitioning plays an additional role

678 to scale mitotic chromosomes to spindle and cell size specifically during metaphase. Consistent

679 with this temporal separation of developmental cues, condensin I acts as a scaling factor only in

680 the N/C pathway and not the importin α pathway (Figure 5C vs. Figure 6D). Together, these data

681 suggest that the NLS-containing cargo that scale mitotic chromosomes, unlike cargo that scale

682 nuclei and spindles, cannot freely exchange with other factors in the egg cytoplasm to lengthen

683 short embryo chromosomes. Future work will be required to identify this cargo. Finally, since

684 *Xenopus* embryos divide asymmetrically, with larger cells on the vegetal side, our results suggest

685 that within the same embryo, the importin α and N/C ratio pathways could combine to have

686 different effects on mitotic chromosome size.

687

688 <u>Multiple molecular pathways can regulate mitotic chromosome size.</u> Based on *in silico* models of

689 condensin I loop extrusion activity, it was predicted that changing condensin I occupancy on

690 mitotic chromosomes causes major changes in DNA loop size and chromosome dimensions

27

691   (Goloborodko et al., 2016). However, it was unclear whether such changes occur *in vivo*. Our

692   results suggest that within the physiologically relevant range of condensin I concentrations

693   present during embryogenesis, less condensin I correlates with both increased loop size and

694   increased length-wise compaction. Another recent study showed that H1.8 can suppress

695   condensin I occupancy on sperm mitotic chromosomes, reducing their length (Choppakatla et al.,

696   2021). In contrast, we found that an increase in condensin I could act independently of H1.8 to

697   lengthen chromosomes (Figure 3-S3), suggesting that condensin I is the major scaling factor for

698   mitotic chromosomes. In the future it will be interesting to examine other factors that could be

699   acting upstream or downstream of condensin I to set mitotic chromosome size in the embryo.

700

701   <u>N/C ratio as a fundamental mechanism for regulating chromatin structure during pre-ZGA</u>

702   <u>cleavage divisions.</u> Previous work in zebrafish and frogs suggested that titration of maternal

703   factors such as histone H3 due to increasing N/C ratio plays an important role in regulating timing

704   of Zygotic Genome Activation (ZGA) in the embryo (Amodeo et al., 2015; Joseph et al., 2017).

705   One proposed model is that decreasing histone abundance facilitates the binding of transcription

706   activation machinery (Joseph et al., 2017). Here we were able to recapitulate this titration effect

707   by simply increasing the concentration of nuclei in egg extracts (Figure 5) and found that N/C ratio

708   is sufficient to regulate mitotic chromosome size but not spindle or nuclear size. Together these

709   results suggest that N/C ratio could be a universal mechanism for regulating chromatin structure

710   across the cell cycle, but for completely different functions: transcriptional regulation during

711   interphase and chromosome segregation during metaphase. In the future it will be interesting to

712   identify additional factors that are titrated from maternal cytoplasm, and how this affects overall

713   chromatin architecture and functions leading up to ZGA.

714

715

716

717 **Materials and methods**

718 <u>Whole embryo immunofluorescence</u>

719 Eggs were fertilized and successfully dividing embryos were fixed in MAD (2 parts methanol, 2

720 parts acetone, 1 part DMSO) at 5-minute intervals at each stage when mitosis was likely to be

721 occurring. After 1-3 hours of fixation, embryos were transferred to fresh MAD before storing at -

722 20 ˚C for up to 3 months. Embryos were then gradually rehydrated into 0.5x SSC (75 mM NaCl,

723 7.5 mM sodium citrate, pH 7.0), bleached in 2% H_2O_2, 5% formamide and 0.5x SSC under direct

724 light or 2-3 hours. Bleached embryos were blocked in 1x PBS, 0.1% Triton X-100, 2 mg/mL BSA,

725 10% goat serum, 5% DMSO for 16-24 hours at 4 ˚C. Primary antibodies were incubated at 2-10

726 µg/mL at 4 ˚C for 60 hours, washed in PBT (1x PBS, 0.1% Triton X-100, 2 mg/mL BSA) for 30

727 hours. Secondary antibodies were added at 2 µg/mL, covered from light and incubated for 60

728 hours at 4 ˚C before washing for 30 hours with PBT. Embryos were then gradually rehydrated into

729 100% methanol, stored overnight at -20 ˚C, then cleared with Murrays solution (2 parts benzyl

730 benzoate, 1 part benzyl alcohol). Embryos were imaged with 20x or 40x objective on Zeiss LSM

731 780 confocal microscope. Once cells containing a mitotic spindle were identified, z-stacks were

732 taken. Using Imaris, we performed 3D visualization and segmentation of mitotic spindles and

733 metaphase plates to directly measure volumes. Cell size was measured in FIJI by manually

734 tracing the cell in the z-stack where the spindle appeared the largest. We used this cell area

735 measurement to calculate cell diameter. Interphase data were calculated using a published

736 dataset (Jevtić and Levy, 2015), which used very similar methods to obtain measurements of

737 nuclear size and cell size.

738

739 <u>Embryo extract preparation and sample reactions</u>

740 *Mitotic embryo extracts.* Stage 3 and stage 8 mitotic embryo extracts were prepared as previously

741 described (Wilbur and Heald, 2013). Briefly, eggs from at least 2 separate females were fertilized

742   synchronously with ~1/2 of a fresh testes. After the appropriate amount of growth at 23 ˚C (1 hour

743   and 45 minutes for stage 3 extract and 5.5 hours for stage 8 extracts), successfully dividing

744   embryos were collected in 2 mL test tubes, washed with 5 times with XB (10 mM Hepes pH 7.8,

745   1 mM MgCl$_2$, 0.1 mM CaCl$_2$, 100 mM KCl, 50 mM sucrose) and 5 times with CSF-XB (10 mM

746   Hepes pH 7.8, 2 mM MgCl$_2$, 0.1 mM CaCl$_2$, 100 mM KCl, 50 mM sucrose, 5 mM EGTA) containing

747   protease inhibitors LPC (10 μg/mL leupeptin, pepstatin and chymostatin). Cytochalasin B (Cyto

748   B) was added in the final wash for a final concentration of 20 μg/mL. Embryos were gently pelleted

749   in a tabletop microcentrifuge at 1,000 rpm for 1 minute, then 2,000 rpm for 30 seconds. Embryos

750   were then crushed in a swinging bucket rotor (Sorvall HB-6) at 10,200 rpm for 12 minutes at 16

751   ˚C. Cytoplasm was removed, placed on ice and immediately supplemented with 10 μg/mL LPC,

752   20 μg/mL CytoB, 1x energy mix (3.75 mM creatine phosphate, 0.5 mM ATP, 0.05 mM EGTA, 0.5

753   mM MgCl$_2$), 0.25 μM cyclinBΔ90 and 5 μM UbcH10 C114S to induce metaphase arrest, and

754   0.6 μM rhodamine-labeled tubulin to visualize microtubules.

755

756   To examine endogenous mitotic chromosomes, 25-100 μL samples of embryo cytoplasm were

757   incubated at 20 ˚C for ~1 hour or until spindles had formed. Samples were diluted 4-fold in CDB

758   (250 mM sucrose, 10 mM Hepes pH 8.0, 0.5 mM EGTA, 200 mM KCl, 1 mM MgCl$_2$) for 5-10

759   minutes, then diluted an additional 5-fold in CFB (5 mM Hepes pH 7.8, 0.1 mM EDTA, 100 mM

760   NaCl, 2 mM KCl, 1 mM MgCl$_2$, 2 mM CaCl$_2$, 0.5% Triton X-100, 20% glycerol and 2%

761   formaldehyde). Chromosomes were then layered on a 5 mL of CCB (5 mM Hepes pH 7.8, 0.1

762   mM EDTA, 100 mM NaCl, 2 mM KCl, 1 mM MgCl$_2$, 2 mM CaCl$_2$ 40% glycerol) and centrifuged

763   onto coverslips at 5500 rpm (HB-6) for 20 minutes. Coverslips were removed and additionally

764   fixed for 5 minutes in ice-cold methanol, and washed 5 times in 1x PBS, 0.1% NP-40 before

765   moving on to immunostaining.

766

767   *Interphasic embryo extracts*. Embryos were first arrested in G2 using 150 μg/mL cycloheximide

768   for 1.5 hours, then washed with ELB (250 mM sucrose, 50 mM KCl, 2.5 mM MgCl2, 10 mM Hepes

769   pH 7.8) containing 10 μg/mL LPC, 200 μg/mL CytoB. Embryos were gently pelleted, then

770   manually crushed with a pestle for 30 seconds before centrifuging at 10,000 g for 10 minutes.

771   Cytoplasm was removed, placed on ice and immediately supplemented with 10 μg/mL LPC, 20

772   μg/mL CytoB, 1x energy mix, and 8% glycerol. Samples were aliquoted and flash frozen and

773   stored at -80°C for up to 2 years. For immunofluorescence, embryo nuclei were thawed and

774   directly fixed in ELB supplemented with 15% glycerol and 2.6% paraformaldehyde for 15 minutes

775   with rocking at room temperature. Fixed nuclei were layered over a 5 mL cushion containing 100

776   mM KCl, 1 mM MgCl$_2$, 100 µM CaCl$_2$, 0.2 M sucrose, and 25% glycerol. Nuclei were spun onto

777   coverslips at 1,000 g for 15 minutes at 16 °C. Coverslips additionally fixed and washed as

778   described above.

779

780   *Western blots.* Stage 3 and stage 9 embryo extracts were prepared as described above and

781   analyzed by Bradford to determine total protein concentrations. 25 μg protein was loaded per

782   sample on 4-20% gradient gels (BioRad). Proteins were transferred overnight at 4 degrees onto

783   nitrocellulose membranes, blocked in 5% milk in Tris Buffered Saline containing 0.1% Triton-X100

784   (TBST) for 1 hour at room temperature, then stained with primary antibodies for 1 hour at room

785   temperature. After washing with PBST 5 times, blots were incubated with secondary antibodies

786   containing infrared dyes for 1 hour at room temperature. After a final wash in PBST, blots were

787   visualized on an LiCor Odyssey Imager.

788

789   <u>Egg extract preparation and sample reactions</u>

790   Egg extracts from *X. laevis* were prepared as previously described (Maresca and Heald, 2006)

791   For crude extracts, eggs were packed in a clinical centrifuge and crushed in an HB6 rotor for 16

792   minutes at 10,200 rpm. The cytoplasm was removed and supplemented with 10 μg/mL LPC, 20

793   μg/mL CytoB, 1x energy mix, and 0.6 μM rhodamine-labeled tubulin. For clarified extracts, crude

794   extracts were centrifuged at 55,000 rpm for 2 hours, and then 30 minutes to pellet membranes (

795   all steps at 4 °C). Supernatants containing soluble fraction of the cytoplasm were flash frozen and

796   stored at -80 °C for up to 3 years.

797

798   *Nuclei reactions and spin downs.* Freshly prepared egg extracts were aliquoted into 20 μL

799   reactions and sent into interphase with addition of 1x CA (0.4 mM $CaCl_2$, 10 mM KCl, 0.1 mM

800    $MgCl_2$). After 5 minutes, sperm nuclei were added at 1000 nuclei/μL unless otherwise specified.

801   Once nuclei had swollen, they were fixed and processed for immunofluorescence as stated above

802   for embryo nuclei.

803

804   *Mitotic chromosome reactions and spin downs.* To form mitotic chromosomes from replicated

805   sperm nuclei, purified sperm nuclei were added to 20 μL of interphase egg extract at 1000

806   nuclei/μL unless otherwise specified. After nuclei had swelled and chromatin was replicated

807   (around 45 minutes), 30 μL fresh metaphase egg extract was added and spindles formed after

808   ~45 minutes. To form mitotic chromosomes from stage 8 G2-arrested embryo nuclei, nuclei were

809   first thawed on ice for 15 minutes before adding 1.5 mL of CSF-XB containing 10 μg/mL LPC.

810   Nuclei were pelleted at 1600 g for 5 minutes at 4 °C. Nuclei pellets were resuspended in 10-15

811   μL of fresh CSF-XB (+LPC), and added at 1000 nuclei/μL to metaphase egg extracts, and mitotic

812   spindles formed within 1 hour. Once successful formation of mitotic spindles and chromosome

813   condensation was confirmed by taking a small sample and staining with Hoechst (1 μg/mL),

814   samples were diluted 100-fold and fixed at the same time in ice-cold 1x XBE2 (5 mM Hepes pH

815   7.8, 100 mM KCl, 2 mM $MgCl_2$, 0.1 mM $CaCl_2$, 5 mM EGTA, 50 mM sucrose) containing 0.25%

816   Triton X-100 and 2% formaldehyde. Fixed chromosomes were layered over a 5 mL cushion

817   containing 1x XBE2 and 30% glycerol and spun onto coverslips at 5500 rpm for 20 minutes at 16

818   ˚C.

819

820   *Mitotic spindle spin downs.* To fix and spin down mitotic spindles instead of mitotic chromosomes,

821   the same procedure was used except spindles were fixed in 1x BRB80 (80 mM PIPES pH 6.8, 1

822   mM $MgCl_2$, 1 mM EGTA) containing 30% glycerol and 0,5% Triton X-100 and cushion buffer

823   contained 1x BRB80 and 40% glycerol.

824

825   *Anaphase reactions*. Once mitotic spindles had formed, reactions were transferred to fresh tubes

826   and 1x CA was added. After 40 minutes of interphase, an additional 0.5x CA was added to ensure

827   full replication of DNA. Successful reactions were confirmed by staining a small sample with

828   Hoechst. After 75 minutes of interphase, nuclei were swollen and an equal volume of fresh

829   metaphase extracts were added to form a second round of metaphase spindles. Once formed,

830   mitotic chromosomes were fixed and isolated using same procedures as described above.

831

832   *Titration experiments.* Anytime nuclei concentration in egg extracts was varied, the volume of

833   extract fixed was also varied to keep the nuclei concentration per coverslip constant. We found

834   this to be important for ensuring that any effects we observed were not due to titration of the

835   antibody used for immunostaining.

836

837   *Importin α experiments.* These experiments were performed as described previously (Brownlee

838   and Heald, 2019). Briefly, extracts were incubated with either DMSO or 10 μM palmostatin for 45

839   minutes at 20˚C before using. Exogenous importin α (WT and NP) was purified from E. coli using

840   previously published constructs and procedures (Brownlee and Heald, 2019).

841

842 Immunofluorescence, imaging and analysis of chromosomes, spindles and nuclei from extracts

843 Once mitotic chromosomes, nuclei or spindles were fixed and isolated on coverslips, they were

844 blocked overnight with 1x PBS, 3% BSA at 4 ˚C. Primary antibodies were added at 1μg/mL 2.5

845 μg/mL for 1 hour at room temperature and washed 5 times with 1x PBS, 0.1% NP-40. Secondary

846 antibodies were added at 1 μg/mL for 1 hour, washed 5 times, then stained with Hoechst at 1

847 μg/mL for 10 minutes. Coverslips were washed two more times, then mounted using Vectashield

848 without DAPI. Imaging was performed on an Olympus BX51 upright epifluorescence microscope

849 using an Olympus PlanApo 60x oil objective for chromosomes and 40x air objective for nuclei and

850 spindles. Images were analyzed in FIJI. Single chromosomes were manually selected and

851 cropped from the rest of the image. Chromosome lengths were measured manually using the

852 freehand line tool. Median intensity values were used to perform background subtractions in each

853 channel and the abundance of a certain factor of interest was calculated by dividing the

854 background-subtracted fluorescence intensity of the factor by the background-subtracted

855 fluorescence intensity of Hoechst.

856

857 Hi-C and contact probability analysis

858 *Preparation of samples and sequencing.* Hi-C was performed as previously described(Belaghzal

859 et al., 2017). Mitotic chromosomes from either replicated sperm or stage 8 embryo nuclei were

860 formed in 250 μL egg extract reactions containing 4000 nuclei/μL. Reactions were then diluted

861 48-fold in XBE2 containing 1% formaldehyde and 0.25% triton X-100. After 10 minutes of fixation

862 with rocking at room temperature, samples were quenched for 5 minutes with 140 mM glycine

863 before transferring to ice for 15 minutes. Chromatin was pelleted at 6,000 g for 20 minutes at 4˚C,

864 then resuspended in XBE2 containing 0.25% Triton X-100. Briefly, pallets were homogenized

865 treated with 0.1% SDS (final concentration) and quenched with 1% Triton X-100 (final

866 concentration) prior to overnight digestion with 400 U DpnII at 37 ˚C. Next day, enzyme was

867   inactivated prior to biotin-fill with biotin-14-dATP for 4 hr at 23 °C. Subsequently, chromatin was

868   ligated at 16 °C for 4 hours. After crosslinking was reversed by proteinase K at 65°C overnight.

869   Sonicated ligation products were size selected for 100-350 bp products. Size selected products

870   were end repaired followed by biotin-pull down with streptavidin. Prior to Illumina Truseq adapter

871   ligation purified DNA fragments were A-tailed. PCR amplification and primer removal were last

872   steps before final library was sequenced on Illumina HiSeq 4000 with PE50.

873

874   *Hi-C analysis.* Hi-C libraries processed by mapping to the *X. Laevis* 10 genome using the distiller

875   pipeline (https://github.com/open2c/distiller-nf). Reads were aligned with bwa-mem, uniquely

876   mapped reads were further processed after duplicate removal. Valid pair reads were binned at 1,

877   2, 5, 10, 25, 50, 100, 250, 500, and 1000kb in contact matrices in the cooler format (Abdennur

878   and Mirny, 2019). Cooler files were normalized using Iternative balancing correction(Imakaev et

879   al., 2012), excluding first two diagonals to avoid artifacts at short range.

880

881   *Hi-C contact probability analysis.* For contact probabilities balanced Hi-C data binned at 1kb was

882   used to calculate contact frequency as function of genomic distance. From cooltools

883   expected_cis, logbin_expected, and combined_binned_expected was used to generate average

884   contact decay plots genome-wide (Venev et al. 2022). First, the contact frequency by distance for

885   each chromosome was calculated using expected_cis. Data was grouped into log spaced bins

886   with logbin_expected. Genome-wide average was calculated by combined_binned_expected.

887

888   **Statement of Competing Interests**

889   We have no competing interests.

890

891

892

893 **Acknowledgements**

900

901
902 **References**

903 Abdennur N, Mirny LA. 2019. Cooler: scalable storage for Hi-C data and other genomically
904 labeled arrays. *Bioinform Oxf Engl* 36:311–316. doi:10.1093/bioinformatics/btz540

905 Amodeo AA, Jukam D, Straight AF, Skotheim JM. 2015. Histone titration against the genome
906 sets the DNA-to-cytoplasm threshold for the Xenopus midblastula transition. *Proc National*
907 *Acad Sci* 112:E1086–E1095. doi:10.1073/pnas.1413990112

908 Belaghzal H, Dekker J, Gibcus JH. 2017. Hi-C 2.0: An optimized Hi-C procedure for high-
909 resolution genome-wide mapping of chromosome conformation. *Methods* 123:56–65.
910 doi:10.1016/j.ymeth.2017.04.004

911 Brownlee C, Heald R. 2019. Importin α Partitioning to the Plasma Membrane Regulates
912 Intracellular Scaling. *Cell* 176:805-815.e8. doi:10.1016/j.cell.2018.12.001

913 Chen P, Tomschik M, Nelson KM, Oakey J, Gatlin JC, Levy DL. 2019. Nucleoplasmin is a
914 limiting component in the scaling of nuclear size with cytoplasmic volume. *J Cell Biol*
915 218:4063–4078. doi:10.1083/jcb.201902124

916 Choppakatla P, Dekker B, Cutts EE, Vannini A, Dekker J, Funabiki H. 2021. Linker histone H1.8
917 inhibits chromatin binding of condensins and DNA topoisomerase II to tune chromosome
918 length and individualization. *Elife* 10. doi:10.7554/elife.68918

919 Dekker FJ, Rocks O, Vartak N, Menninger S, Hedberg C, Balamurugan R, Wetzel S, Renner S,
920 Gerauer M, Schölermann B, Rusch M, Kramer JW, Rauh D, Coates GW, Brunsveld L,
921 Bastiaens PIH, Waldmann H. 2010. Small-molecule inhibition of APT1 affects Ras
922 localization and signaling. *Nat Chem Biol* 6:449–456. doi:10.1038/nchembio.362

923 Ganji M, Shaltiel IA, Bisht S, Kim E, Kalichava A, Haering CH, Dekker C. 2018. Real-time
924 imaging of DNA loop extrusion by condensin. *Science* 360:102–105.
925 doi:10.1126/science.aar7831

926 Gibcus Johan H., Samejima K, Goloborodko A, Samejima I, Naumova N, Kanemaki M, Xie L,
927   Paulson JR, Earnshaw WC, Mirny LA, Dekker J. 2018. Mitotic chromosomes fold by
928   condensin-dependent helical winding of chromatin loop arrays. *Biorxiv* 174649.
929   doi:10.1101/174649

930 Gibcus Johan H, Samejima K, Goloborodko A, Samejima I, Naumova N, Nuebler J, Kanemaki
931   MT, Xie L, Paulson JR, Earnshaw WC, Mirny LA, Dekker J. 2018. A pathway for mitotic
932   chromosome formation. *Science* 5:eaao6135. doi:10.1126/science.aao6135

933 Goloborodko A, Imakaev MV, Marko JF, Mirny L. 2016. Compaction and segregation of sister
934   chromatids via active loop extrusion. *Elife* 5:11202. doi:10.7554/elife.14864

935 Good MC, Vahey MD, Skandarajah A, Fletcher DA, Heald R. 2013. Cytoplasmic volume
936   modulates spindle size during embryogenesis. *Science* 342:856–860.
937   doi:10.1126/science.1243147

938 Hara Y, Iwabuchi M, Ohsumi K, Kimura A. 2013. Intranuclear DNA density affects chromosome
939   condensation in metazoans. *Mol Biol Cell* 24:2442–2453. doi:10.1091/mbc.e13-01-0043

940 Hazel J, Krutkramelis K, Mooney P, Tomschik M, Gerow K, Oakey J, Gatlin JC. 2013. Changes
941   in Cytoplasmic Volume Are Sufficient to Drive Spindle Scaling. *Science* 342:853–856.
942   doi:10.1126/science.1243110

943 Heald R, Gibeaux R. 2018. Subcellular scaling: does size matter for cell division? *Curr Opin Cell*
944   *Biol* 52:88–95. doi:10.1016/j.ceb.2018.02.009

945 Imakaev M, Fudenberg G, McCord RP, Naumova N, Goloborodko A, Lajoie BR, Dekker J, Mirny
946   LA. 2012. Iterative correction of Hi-C data reveals hallmarks of chromosome organization.
947   *Nat Methods* 9:999–1003. doi:10.1038/nmeth.2148

948 Jevtić P, Levy DL. 2015. Nuclear size scaling during Xenopus early development contributes to
949   midblastula transition timing. *Curr Biol* 25:45–52. doi:10.1016/j.cub.2014.10.051

950 Joseph SR, Pálfy M, Hilbert L, Kumar M, Karschau J, Zaburdaev V, Shevchenko A,
951   Vastenhouw NL. 2017. Competition between histone and transcription factor binding
952   regulates the onset of transcription in zebrafish embryos. *Elife* 6. doi:10.7554/elife.23326

953 Kieserman EK, Heald R. 2014. Mitotic chromosome size scaling in Xenopus. *Cell Cycle*
954   10:3863–3870. doi:10.4161/cc.10.22.17975

955 Kletter T, Reusch S, Cavazza T, Dempewolf N, Tischer C, Reber S. 2021. Volumetric
956   morphometry reveals spindle width as the best predictor of mammalian spindle scaling. *J*
957   *Cell Biology* 221:e202106170. doi:10.1083/jcb.202106170

958 Kramer EM, Tayjasanant PA, Cordone B. 2021. Scaling Laws for Mitotic Chromosomes. *Front*
959   *Cell Dev Biol* 9:684278. doi:10.3389/fcell.2021.684278

960 Ladouceur A-M, Dorn JF, Maddox PS. 2015. Mitotic chromosome length scales in response to
961   both cell and nuclear size. *J Cell Biol* 209:645–651. doi:10.1083/jcb.201502092

962 Ladouceur A-M, Ranjan R, Smith L, Fadero T, Heppert J, Goldstein B, Maddox AS, Maddox PS.
963   2017. CENP-A and topoisomerase-II antagonistically affect chromosome length. *J Cell Biol*
964   216:2645–2655. doi:10.1083/jcb.201608084

965 Levy DL, Heald R. 2015. Biological Scaling Problems and Solutions in Amphibians. *Cold Spring*
966   *Harb Perspect Biol* 8:a019166. doi:10.1101/cshperspect.a019166

967 Levy DL, Heald R. 2010. Nuclear size is regulated by importin α and Ntf2 in Xenopus. *Cell*
968   143:288–298. doi:10.1016/j.cell.2010.09.012

969 Maresca TJ, Freedman BS, Heald R. 2005. Histone H1 is essential for mitotic chromosome
970   architecture and segregation in Xenopus laevis egg extracts. *J Cell Biol* 169:859–869.
971   doi:10.1083/jcb.200503031

972 Maresca TJ, Heald R. 2006. Methods for studying spindle assembly and chromosome
973   condensation in Xenopus egg extracts. *Methods Mol Biol* 322:459–474. doi:10.1007/978-1-
974   59745-000-3_33

975 Micheli G, Luzzatto AR, Carrì MT, Capoa A de, Pelliccia F. 1993. Chromosome length and DNA
976   loop size during early embryonic development of Xenopus laevis. *Chromosoma* 102:478–
977   483.

978 Nand A, Zhan Y, Salazar OR, Aranda M, Voolstra CR, Dekker J. 2021. Genetic and spatial
979   organization of the unusual chromosomes of the dinoflagellate Symbiodinium
980   microadriaticum. *Nat Genet* 53:618–629. doi:10.1038/s41588-021-00841-y

981 Naumova N, Imakaev M, Fudenberg G, Zhan Y, Lajoie BR, Mirny LA, Dekker J. 2013.
982   Organization of the mitotic chromosome. *Science* 342:948–953.
983   doi:10.1126/science.1236083

984 Neurohr G, Naegeli A, Titos I, Theler D, Greber B, Díez J, Gabaldón T, Mendoza M, Barral Y.
985   2011. A midzone-based ruler adjusts chromosome compaction to anaphase spindle length.
986   *Science* 332:465–468. doi:10.1126/science.1201578

987 Nielsen CF, Zhang T, Barisic M, Kalitsis P, Hudson DF. 2020. Topoisomerase IIα is essential for
988   maintenance of mitotic chromosome structure. *Proc Natl Acad Sci USA* 117:12131–12142.
989   doi:10.1073/pnas.2001760117

990 Schubert I, Oud JL. 1997. There is an upper limit of chromosome size for normal development
991   of an organism. *Cell* 88:515–520.

992 Shintomi K, Hirano T. 2011. The relative ratio of condensin I to II determines chromosome
993   shapes. *Genes Dev* 25:1464–1469. doi:10.1101/gad.2060311

994 Sullivan W, Daily DR, Fogarty P, Yook KJ, Pimpinelli S. 1993. Delays in anaphase initiation
995   occur in individual nuclei of the syncytial Drosophila embryo. *Mol Biol Cell* 4:885–896.

996 Wilbur JD, Heald R. 2013. Mitotic spindle scaling during Xenopus development by kif2a and
997   importin α. *Elife* 2:e00290. doi:10.7554/elife.00290

998   Wühr M, Chen Y, Dumont S, Groen AC, Needleman DJ, Salic A, Mitchison TJ. 2008. Evidence
999   for an upper limit to mitotic spindle length. *Curr Biol* 18:1256–1261.
1000   doi:10.1016/j.cub.2008.07.092

1001